# EXPERIMENTAL DEFORMATION OF O+ ORIENTED SYNTHETIC QUARTZ SINGLE CRYSTALS

A Thesis

Presented to

The Graduate Faculty of The University of Akron

In Partial Fulfillment

of the Requirements for the Degree

Master of Science

Edward J. Poston

May, 2017

EXPERIMENTAL DEFORMATION OF O+ ORIENTED SYNTHETIC QUARTZ SINGLE CRYSTALS

Edward J. Poston

Thesis

Approved:

Advisor
Dr. Caleb W. Holyoke, III

Faculty Reader
Dr. LaVerne M. Friberg

Faculty Reader
Dr. John A. Peck

Interim Department Chair
Dr. Stephen C. Weeks

Accepted:

Interim Dean of the College
Dr. John Green

Dean of the Graduate School
Dr. Chand Midha

Date

## ABSTRACT

A Griggs rig apparatus was used to perform a number of strain rate stepping and pressure stepping experiments of O+ oriented synthetic quartz crystals. These samples were annealed at 1 atm and 900°C for 24 hours to convert the gel type water inclusions to free water inclusions similar to those that are found in natural milky quartz. Strain rate stepping experiments were performed at temperatures from 1000°C to 750°C, and strain rates from 1.6 X $10^{-4}$ $s^{-1}$ to 1.6 X $10^{-6}s^{-1}$, while confining pressure was held constant at 1.5 GPa. These samples were observed to yield over a range of <10 to ~300 MPa in many cases, though under some of the conditions tested samples did not yield. Two pressure stepping experiments were performed, one at 800°C and one at 750°C, with a strain rate of 1.6 X $10^{-6}s^{-1}$ and confining pressures between 0.6 GPa and 1.5 GPa. The sample strengths measured in the pressure stepping experiments were between ~30 MPa and ~60 MPa. Microstructures observed within deformed samples include undulatory extinction and deformation lamellae. The mechanical data from those experiments that were consistent with dislocation creep fit the flow law:

$$\dot{\varepsilon}=0.00177*C_{H_2O}^{1.9}*f_{H_2O}*\sigma_{diff}^{3.29}*e^{(-268.6/(R*T))}$$

Under natural conditions, this suggests plastic yielding of quartz occurs at ~9 km (~225°C) deep in the crust.

ACKNOWLEDGEMENTS

I would like to thank Dr. Caleb Holyoke, my advisor for this thesis, as well as Steve Kirby of the USGS for the quartz crystal used in this study and the National Science Foundation for the grant (EAR-1321882, given to C. Holyoke and A. Kronenberg) that provided funding for my study.

TABLE OF CONTENTS

Page

LIST OF FIGURES

LIST OF TABLES

# CHAPTER I

# INTRODUCTION

Quartz is one of the most common minerals in the continental crust and is likely one of the most important minerals in determining the continental crust's strength. In natural settings, quartz is frequently the weakest mineral present, and as such is often the first mineral to yield plastically in continental crust (Kohlstedt et al., 1995). The weakness of quartz in the crust is evident from the structures seen in studies of naturally deformed quartz rich rocks (Hacker et al., 1990; Stipp et al., 2002). Because of the fact that quartz is both abundant and weak in the continental crust, wet quartz (which contains water in fluid inclusions) undergoing plastic deformation will determine where the crust transitions from brittle deformation to ductile deformation, and how the crust responds to stresses.

Naturally deformed rocks can give some indication as to the conditions they were under when they were deformed through an analysis of the microstructures and minerals present in the rocks. However, in order to determine the relation between quartz microstructures and deformation conditions more precise information must be available. This information can be gathered by experimentally deforming either rocks or individual minerals in order to measure at which conditions they experience the different stages of deformation. While deformation experiments cannot reasonably be performed at geologic strain rates, previous studies have shown that by increasing the temperature of the experiment, the strain rate can be increased, while the deformation mechanism remains the same. That the deformation mechanism remains the same for both natural

and experimental deformation means that the flow laws developed using experimental data can be extrapolated to describe naturally occurring deformation.

Attempts to deform quartz in laboratory settings, which is necessary to quantitatively describe quartz deformation mechanisms, have been wrought with difficulties. Early laboratory studies were ineffective in experimentally deforming quartz, as the pure, dry material they were using was much stronger than was expected and observed in naturally deformed quartzite (Christie et al., 1964). Griggs and Blacic (1965) discovered that quartz was much weaker in the presence of water, first noticed in experiments using synthetic quartz crystals, which had higher water contents than the pure dry natural material used in initial experiments. They tested the hypothesis that the weakening was caused by water by using talc as a confining medium in experiments on originally dry natural single quartz crystals. The talc provided water that diffused into their samples, weakening them (Griggs et al., 1966). Unfortunately, the mechanical data gathered using talc assemblies cannot be used due to the high strength of the talc assembly obscuring the strength of the quartz (Stewart et al., 2013).

Experiments have been performed using natural milky quartz, but the experiments have issues with a lack of homogeneity in the fluid inclusion distribution (Kekulawala et al., 1978; Kronenberg et al., 2001; Holyoke and Kronenberg, 2013; and Stünitz et al., 2017). The heterogeneous distribution of fluid inclusions in the milky quartz samples lead to highly variable flow strength measurements for milky quartz, and the samples often show heterogeneous deformation bands (Kronenberg et al., 2001). The variability within the samples has made it difficult to use milky quartz to examine relationships in flow law parameters, such as the effects of water fugacity on sample strength (Stünitz et al., 2017).

A more homogeneous material is synthetic single quartz. Experiments have been performed using synthetic quartz (Kekulawala et al., 1981; and Linker et al., 1984), though they rarely reach constant stress/strain rate deformation due to the water changing

from gel-type inclusions to free water fluid inclusion. These experiments using synthetic quartz single crystals have been done at low confining pressures (0.1 MPa, Linker and Kirby, 1981; 300 MPa, Kekulawala et al., 1981). The synthetic quartz in these crystals deformed at ephemeral conditions, not the constant stress/constant strain rate conditions necessary for proper flow law development. The ephemeral conditions resulted in synthetic samples registering as abnormally weak compared to natural quartz, and were shown to be due to the condition of the synthetic quartz crystals, where their deformation occurred concomitant with the precipitation of water into fluid conclusions. The water in synthetic quartz crystals initially is in the form of tiny, unfreezable gel-like inclusions, which do not occur in natural milky quartz. A potential correction for the form of water in synthetic quartz not matching natural crystals is to heat treat the starting material (Kekulawala et al., 1978) which alters the water to form free water fluid inclusions like those observed in natural quartz crystals. Heat treating the starting material may serve to make using synthetic quartz single crystals advantageous over the use of natural milky quartz crystals for deformation.

Data relating strength and strain rate, temperature, and water fugacity also exists for experimental quartzite deformation, both using natural quartzite (commonly Black Hills quartzite) (Hirth and Tullis, 1992; Gleason and Tullis, 1995; Chernak et al, 2009; Holyoke and Kronenberg, 2013) and synthetic quartz aggregates (Luan and Paterson, 1992), but disagreements between the resulting flow laws remain (Figure 1), and good single crystal studies could potentially resolve them. Understanding single crystal deformation may help to better understand how deformation occurs in quartz and separate the contributions of intergranular processes such as dislocation creep from intragranular processes like grain boundary migration. Single crystal deformation also has the advantage of isolating individual slip systems in quartz, allowing determination of a flow law for a specific slip system.

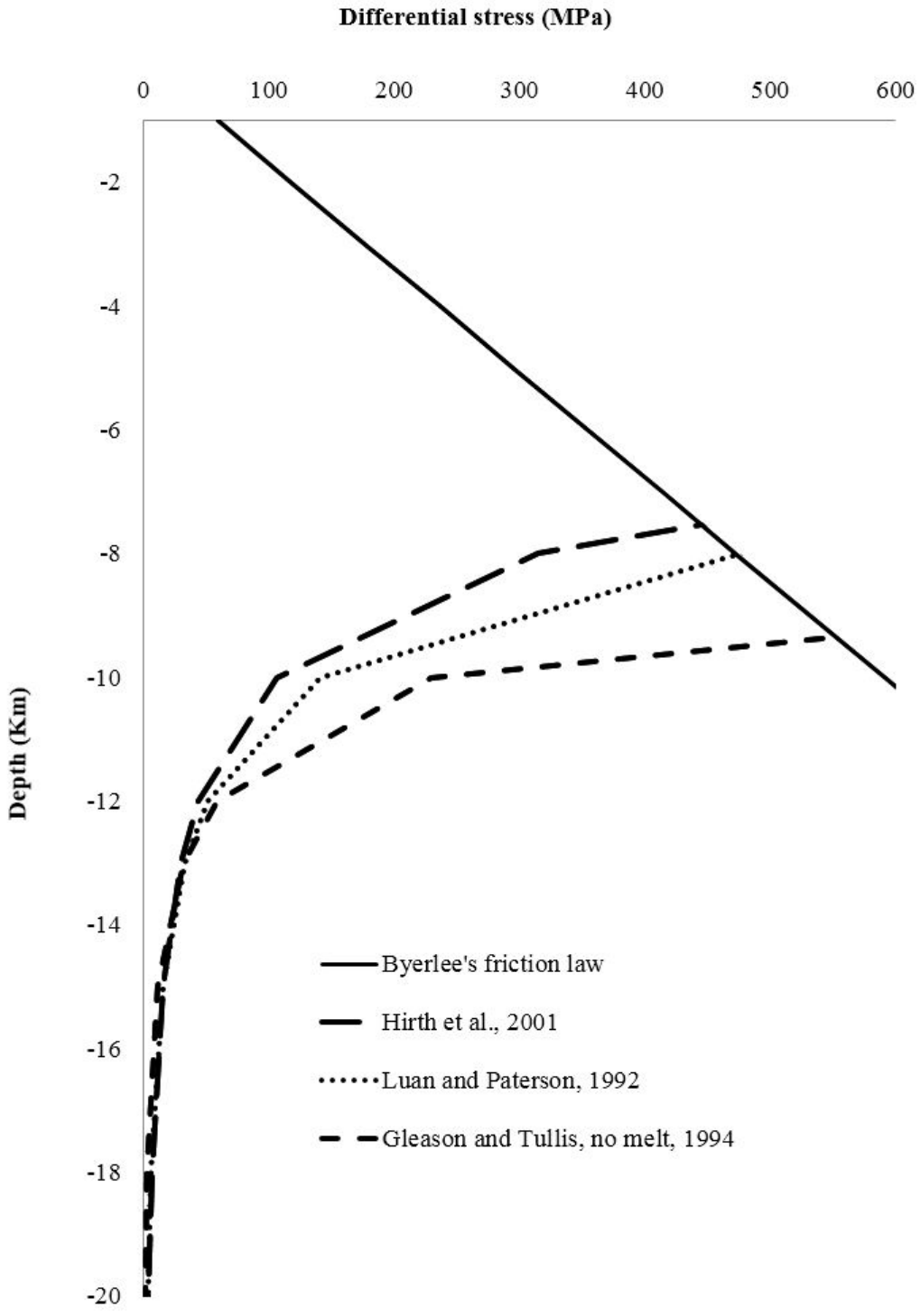


Figure 1. Strength of the lithosphere. The strength of the brittle zone is given by Byerlee's law, while the strength of the ductile zone is given based on the different experimentally determined models for quartzite yield strength (Hirth et al, 2011; Luan and Paterson, 1992; Gleason and Tullis, 1994).

For this study, I examined the deformation of a single quartz crystal orientation (O+) through a series of deformation experiments. These experiments were designed to collect data to establish the stress exponent, activation energy, and any potential effects of water on the strength of quartz for the easy slip direction in quartz. For the O+ orientation in single quartz, the easy slip direction is either basal <a> or prism <c>, which are oriented at 45° to the principle stress direction.

There were a few goals to this study. One goal was to test the hypothesis that synthetic quartz single crystals can be used as starting material and be made to deform by steady state mechanisms. Another goal was to determine which slip system, basal <a> (that is, basal {0001} slip in the a-directions $<2\bar{1}\bar{1}0>$) or prism <c> (that is, slip in the c-direction <0001> on prisms at $\{2\bar{1}\bar{1}0\}$), is the easy slip system and thus deforms for synthetic quartz oriented in the O+ orientation, and possibly find the proportion between the two, should both be activated, with the hypothesis being that the basal <a> slip system would be dominant. A third goal of the study was to derive a flow law for the deformation of quartz single crystals, oriented in the O+ orientation. A hypothesis here is that either higher water content, higher water fugacity, or both would decrease the strength of quartz. A final goal of this study was to examine the microstructures of the deformed samples, in order to understand how the deformation occurred, and check that the deformation mechanism that occurred was that same as is expected to cause quartz deformation in nature; this would help to answer all three of the hypotheses presented here.

# CHAPTER II

# METHODS

In order to understand the deformation of single crystals of quartz, I deformed synthetic quartz single crystals at temperatures from 750°C to 1000°C, strain rates from $10^{-6}$ $s^{-1}$ to $10^{-4}$ $s^{-1}$, and confining pressures from 600 to 1500 MPa. These experiments included those performed at a single confining pressure-temperature-strain rate combination and experiments with deformation steps performed at more than one confining pressure-temperature-strain rate combination. After deformation, these experiments were examined for microstructures consistent with dislocation creep. Additionally, water content was measured for the samples to determine if there was a relationship between water content and sample strengths.

The starting material was a synthetic quartz crystal, X-534-3, provided by Steve Kirby at the United States Geological Survey. Synthetic quartz was used to avoid the high variability of distribution and size of fluid inclusions within a natural milky quartz crystal. 5 mm diameter samples were cored from the crystal in the O+ orientation, which puts the basal <a> and prism <c> slip systems in an easy slip orientation (Figure 3). These cores were cut and the faces ground perpendicular to the length of the cylinders to starting lengths between 9 and 11 millimeters, depending on the amount of deformation planned for the experiment. Following the preparation, a heat treatment step was performed to change the form of water in the synthetic quartz from unfreezable gel-type inclusions into free water fluid inclusions as seen in milky quartz (Kekulawala et al., 1978). The heat treatment was performed at 1 atmosphere pressure and 900°C for ~24

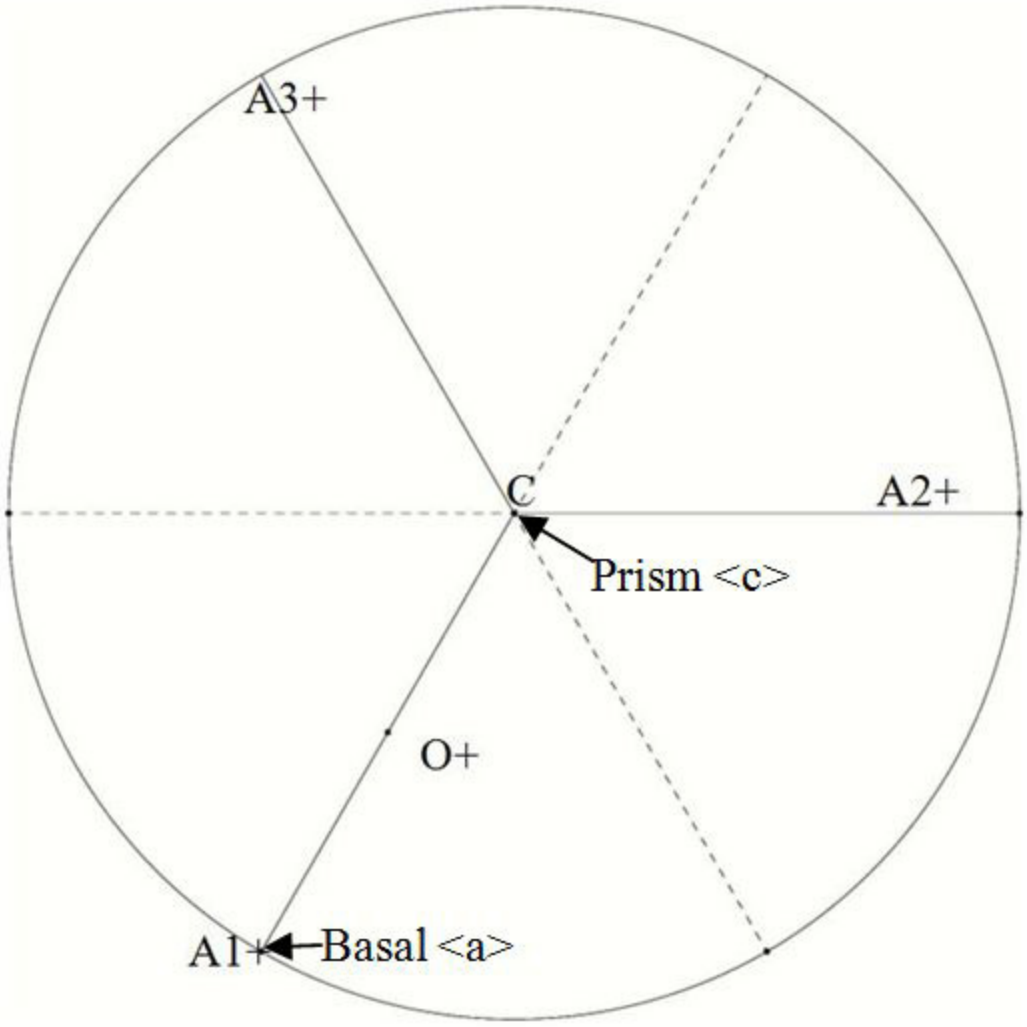


Figure 2. Stereographic projection of a quartz crystal. The coring direction is at the point labeled O+, halfway between the C- and A- axes, which are labeled with their respective slip systems.

hours (Figure 3). The temperature is brought down slowly, which is meant to decrease the chance of the samples developing cracks during the quartz inversion or from thermal cracking. To evaluate the success of this method for changing the water type, Fourier transform infrared (FTIR) measurements were made on discs cut from the ends of the cores used for experiments, both before and after heat treatment, as well as from the sample itself after deformation.

Uniaxial deformation experiments were performed using a Griggs-type piston cylinder deformation apparatus. Four of these experiments were performed using solid salt assemblies (Figure 4b). The temperature was measured near the sample during the experiments using a platinum -platinum 90% rhodium 10% thermocouple (thermocouple type S). Metal jackets were used to isolate the samples from the confining medium. In high temperature experiments (T>850°C) a thick nickel jacket was placed around the sample, followed by a platinum jacket, as well as a set of nickel and platinum discs at the top and bottom, which the platinum jacket was folded over. Outside of the platinum jacket was placed a thin nickel jacket, meant to pin the grain size of the platinum. In lower temperature experiments (T≤850°C), the samples were isolated from the salt using silver foil, discs, and a thin silver jacket instead of the platinum and nickel jackets, because the strength of nickel at those temperatures interferes with accurate data collection. The assemblies were heated using a resistive graphite furnace. Calibration for the differential stress measurements from the molten salt assembly is $0.73*\sigma_{measured}$–50 MPa = $\sigma_{actual}$ (Holyoke and Kronenberg, 2010).

The majority of experiments were performed using a molten salt cell (Figure 4c), in which the confining medium is a eutectic lithium chloride - potassium chloride mixture, which becomes molten at experimental conditions (Holyoke and Kronenberg, 2010). These assemblies were used to improve the data resolution compared to the solid salt cells. To keep the sample isolated from the molten salt confining medium (which

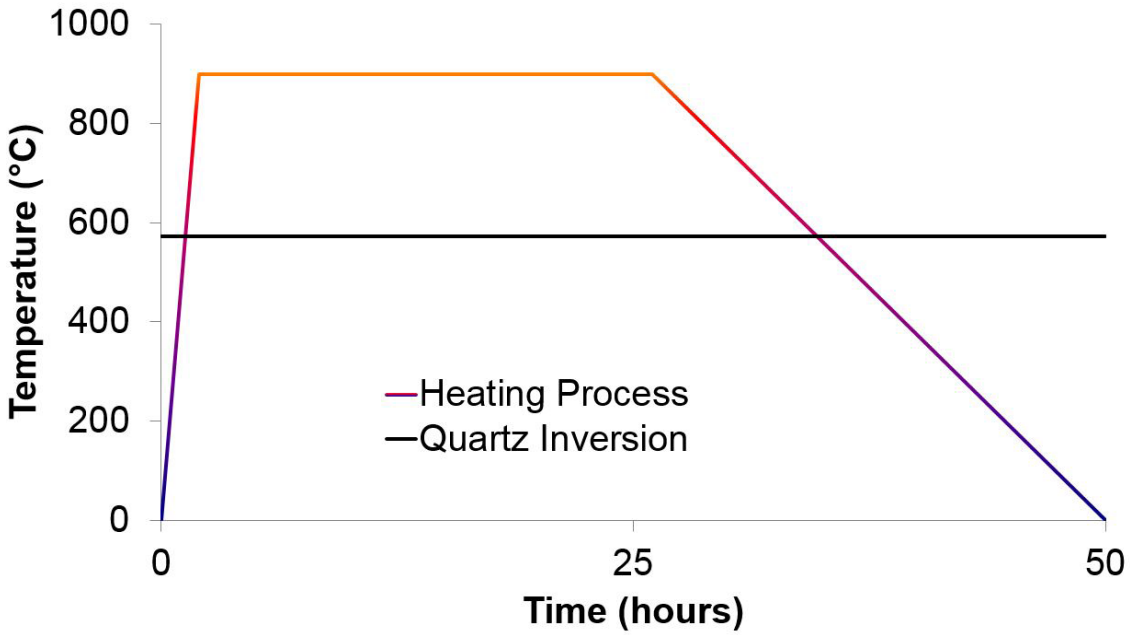


Figure 3. Temperature path during 1 atm annealing process. The black line indicates the temperature for quartz inversion at 1 atm.

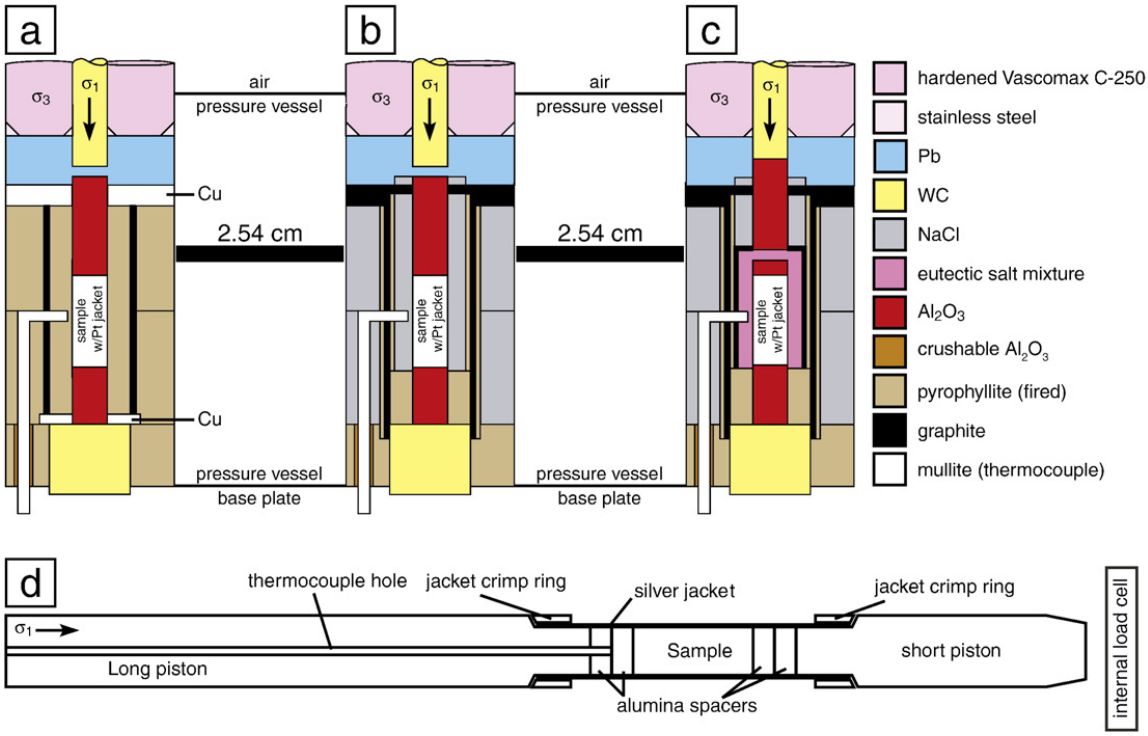


Figure 4. a) Historic assembly using pyrophillite confining medium. (b) Solid salt assembly, as was used for some experiments in this paper. (c) Molten salt assembly, as was used in the rest of the experiments in this paper. (d) Schematic of Heard gas apparatus' load column, used by others. In all cases, the arrow labeled $\sigma_1$ indicates the direction of movement of the load piston. (from Holyoke and Kronenberg, 2010)

dissolves quartz), samples were weld sealed in the platinum jacket. Higher temperature experiments (≥900 C) used the same type of nickel jacket that was used in the solid salt assemblies inside the platinum, while lower temperature experiments (T<900°C) used the silver foil and discs inside the platinum can. A thin nickel jacket was also used, placed around the platinum can to keep the platinum grain size from growing. The assemblies were heated and the temperature measured using the same methods as used in the solid salt cell experiments. Calibration for the differential stress measurements from the molten salt assembly is $0.73*\sigma_{measured} = \sigma_{actual}$ (Holyoke and Kronenberg, 2010).

The sample assembly was placed in a pressure vessel, taken up to pressure and temperature conditions following a standard path. This procedure is to first increase the confining pressure 250 MPa, and then to alternate increasing pressure and temperature (in 100 degree and 100 MPa increments) until the temperature is at 300°C and the confining pressure is 500 MPa, then increase the confining pressure to the value needed for the experiment, and finally increase the temperature to the desired value. Pressure increases are performed at a starting rate of no more than ~200 MPa per hour for the first ~250 MPa, then sped up to between 300 and 400 MPa per hour for the remaining pressure increases. Initial temperature increases occur over a few minutes, with the final temperature increase occurring over roughly 15 minutes. Additionally, the load piston is advanced in order to prevent lead leakage from the top of the assembly into the piston; typically about 1 millimeter after the first temperature step and then about one-eighth of a millimeter every 100 MPa step thereafter.

Gear settings on the Griggs rig allow for different orders of magnitude of strain rate, with available settings of $10^{-4}$/s, $10^{-4.5}$/s, $10^{-5}$/s, $10^{-5.5}$/s, $10^{-6}$ /s (approximately a 20 minute to an 18 hour deformation period), and slower settings which were not used in this study. Following the final deformation step, the piston was retracted so that it would not load the

sample during quenching to ~300°C. The pressure and temperature were then lowered to room conditions over a period of ~1 hour.

Samples were cut open (parallel to $\sigma_1$) following the experiment, in order to create thin and thick FTIR sections. A petrographic microscope was used to examine the microstructures in the thin sections that were produced by the deformation. This was done to confirm that samples remained single crystals and contained microstructures consistent with dislocation creep and that the samples were still single crystals for the most part.

FTIR analyses were performed on thick sections. FTIR spectra were collected using a Nicolet Continuum FT-IR microscope, with 512 scans per spectra. Background spectra were taken at the minimum of once every hour. Water content was measured by FTIR using the method from Stipp et al. (2006), which analyzes the broad band from 3000 to 3780 $cm^{-1}$, caused by O-H vibration and stretching.

# CHAPTER III

# RESULTS

Three types of experiments were performed to determine single crystal quartz mechanical properties: 1) Single deformation step experiments with solid or molten salt assemblies, 2) Strain rate stepping experiments with solid or molten salt assemblies, and 3) pressure stepping experiments in molten salt assemblies. Experiments were performed at strain rates ranging from ~$1.6*10^{-4}$ to $1.6*10^{-6}$ $s^{-1}$, confining pressures of ~650 MPa to 1500 MPa, and temperatures from 750°C to 1000°C. Descriptions of experimental results are discussed below.

## 3.1 Single deformation step experiments

The single deformation step experiments were performed at a strain rate of ~$6.8*10^{-5}$ $s^{-1}$ and confining pressure of 1.5 GPa. The experiments served to determine the microstructures present in samples deformed under only a single set of conditions. Additionally, the experiments were used for comparison of different temperatures on the strength of single quartz crystals.

### 3.1.1 Single deformation step mechanical data

The two experiments Z-30 and Z-34 were performed in solid salt assemblies, because the expected strengths exceeded the desireable upper limit of stresses in the molten salt cell (250 MPa). Z -30 was deformed at T=800°C and Z-34 at T=750°C, and both were performed at a confining pressure of 1.5 GPa and strain rate of $6.8*10^{-5}$ $s^{-1}$ (Figure 5;

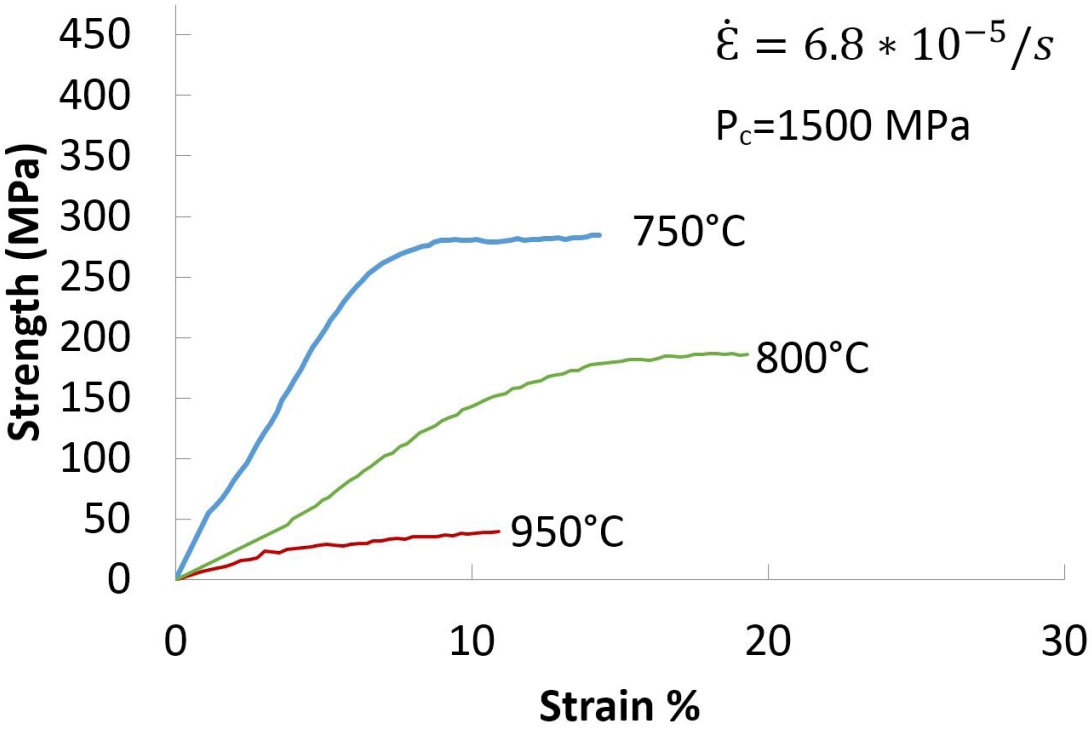


Figure 5. Stress-strain curves for single deformation step experiments Z-29 (red), Z-30 (green), and Z-34 (blue). The samples deformed at lower temperatures experienced a higher differential stress than the samples deformed at higher temperatures.

Table 1. List of experiments and experimental conditions used in this study.

| Experiment | Solid or Molten assembly | Confining Pressure (MPa) | Temperature (°C) | Strain Rate ($s^{-1}$) | Strain % | Strength (MPa) | Water Content ($H/10^6$ Si) | Comments |
|---|---|---|---|---|---|---|---|---|
| Z-2 | Solid | 1500 | 900 | $1.6X10^{-4}$ | 10.07 | 88 | 234 | Fits dataset when corrected for water content |
| | | | | $1.6X10^{-5}$ | 16.18 | 3 | | Probably too weak to be reliable, microstructures include undulatory extinction, deformation lamellae |
| Z-5 | Solid | 1500 | 800 | $1.6X10^{-4}$ | 8.74 | >750 | 432 | Sample shows some recrystallization in the center, probably occurred late in the experiment. |
| | | | | $1.6X10^{-6}$ | 15.37 | 56 | | |
| | | | | $1.6X10^{-5}$ | 22.73 | >600 | | |
| Z-23 | Molten | 1500 | 1000 | $1.6X10^{-4}$ | 6.5 | 7 | 464 | Probably too weak to be reliable |
| | | | 900 | $1.6X10^{-4}$ | 11.03 | 58.4 | | Microstructures: sample shows some undulatory extinction. |
| | | | | $6.8X10^{-5}$ | 14.5 | 40.2 | | |
| | | | | $1.6X10^{-5}$ | 19.22 | 29.2 | | |
| Z-26 | Molten | 1500 | 800 | $1.6X10^{-6}$ | 4.94 | 26 | 393, see comments | Salt leak weakened sample toward end; first step's strength is obscured by confining pressure fluctuations and may not have yielded. Water content is estimated by an average of nearby sample water contents. |
| | | | | $1.6X10^{-5}$ | 16.8 | 140 | | |
| | | | | $6.8X10^{-6}$ | 33.63 | 48 | | |
| Z-28 | Molten | 1500 | 850 | $1.6X10^{-4}$ | 2.2 | >125 | 165 | Undulatory extinction occurs both parallel to and perpendicular to c axis orientation. Sample seems unusually dry compared to others, but also appears stronger than expected. |
| | | | | $1.6X10^{-5}$ | 7 | 106 | | |
| | | | | $6.8X10^{-5}$ | 9.26 | >200 | | |
| | | | | $6.8X10^{-6}$ | 14.5 | 74.5 | | |
| | | | | $1.6X10^{-5}$ | 20.43 | >150 | | |
| Z-29 | Molten | 1500 | 950 | $6.8X10^{-5}$ | 10.92 | 28 | 382 | Undulatory extinction |
| Z-30 | Solid | 1500 | 800 | $6.8X10^{-5}$ | 19.3 | 187 | 523 | Undulatory extinction, fractures (from unloading?) |
| Z-34 | Solid | 1500 | 750 | $6.8X10^{-5}$ | 14.3 | 283 | 720 | Undulatory extinction, fractures (unloading?) Water measurements showed high variability. |
| Z-56 | Molten | 1470 | 800 | $1.8X10^{-6}$ | 5.33 | 49 | 286 | Undulatory extinction (c-axis related), and subgrain formation. |
| | | 910 | | | 11.87 | 46 | | |
| | | 700 | | | 19.77 | 49 | | |
| Z-61 | Molten | 1475 | See comments | $1.8X10^{-6}$ | 4.5 | 33 | See comments | Temperature not constant during this step, kept near 750 |
| | | | 750 | | 9.8 | 33 | | Salt leak weakened sample; sample recovered still somewhat intact, indicating salt leak was likely late in the experiment- water content measurement not taken as a result. |
| | | 900 | | | 16.3 | 47.5 | | |
| | | 680 | | | 20.6 | 58 | | |
| | | 1500 | | | 24 | 28 | | |

Table 1). As expected, the hotter experiment, Z-30, was weaker than the colder one Z-34. Z-30 experienced a rapid increase in differential stress until ~14% strain, and Z-34 behaved similarly up until ~8.5% strain. That period of increasing differential stress represents elastic behavior, which changes to plastic deformation upon yielding. Differential stress upon yielding was ~190 MPa for Z-30 and ~280 for Z-34. Both samples experienced ~5% strain after yielding.

Experiment Z-29 was performed using a molten salt assembly, since it was expected to be too weak to measure in the solid salt assembly. The experiment was performed at a higher temperature (950°C), but had the same confining pressure of 1.5 GPa and strain rate of $6.8*10^{-5}$ $s^{-1}$ that were used for Z-30 and Z-34 (Table 1). Z-29 was weaker than both experiments Z-30 and Z-34, as it was performed at a higher temperature. Experiment Z-29 transitioned from elastic to plastic deformation after ~5% after the initial loading point, and was then strained for about 5% past the point where it yielded, which was at a differential stress of about 28 MPa (Figure 5).

### 3.1.2 Single deformation step microstructures

The microstructures are very similar between the two samples, Z-30 and Z-34. Both, however, are somewhat obscured by extensive fractures, either horizontal or vertical. The horizontal cracks do not contain recrystallized grains, cross all other fractures in the samples, and are consistent with cracks formed by decompression. The vertical cracks contain many small grains, obscuring undulatory extinction within the sample, and there seem to be more water inclusions along these cracks (Figure 6a, b). The vertical cracks are generally parallel to the compression direction and have been observed in some milky quartz single crystal experiments (Stünitz et al., 2017).

The sample Z-29 shows little change when compared with the starting material. It lacks the larger cracks that are present in samples Z-30 and Z-34, and the fluid inclusions

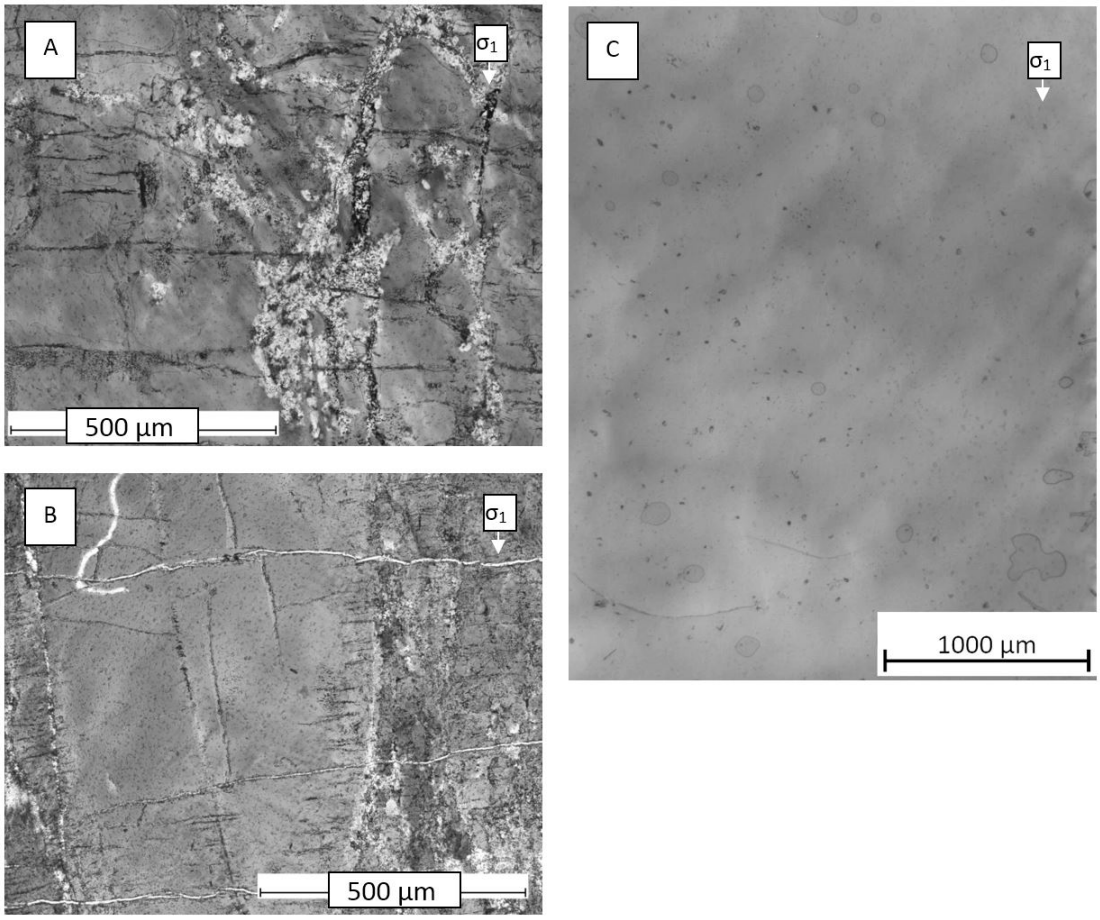


Figure 6. (A) Sample Z-30 (800°C, 19% strain) and (B) Z-34 (750°C, 14% strain). Both A and B show some undulatory extinction, and small amounts of recrystallization along vertical cracks. (C) Sample Z-29 (950°C, 11% strain) shows undulatory extinction. All three experiments were performed at a strain rate of $10^{-4.5}$ $s^{-1}$ and confining pressure of 1.5 GPa. All images were taken using crossed polarized light.

are still randomly distributed throughout the crystal. The sample does however show some slight undulatory extinction (Figure 6c).

## 3.2 Strain-rate stepping experiments

The bulk of experiments performed in this study were strain-rate stepping experiments performed at individual confining pressure and temperature conditions (pressure = 1.5 GPa, temperature = 800°C, 850°C, and 900°C). These experiments were performed to establish the relation between the strength and strain rate in quartz crystals over a range of temperatures. Experiments Z-2 and Z-5 were performed in solid salt assemblies, while Z-23, Z-26, and Z-28 were performed in molten salt assemblies.

### 3.2.1 Solid salt experiments Z-2 and Z-5

Two strain rate stepping experiments were performed in solid salt assemblies, Z-2 and Z-5. Z-2 was run at 900°C and strain rate of $1.6*10^{-4}$ $s^{-1}$. It yielded after about 4% strain in the first step, continuing to ~10% total strain at a differential stress of about 88 MPa (Figure 7). A second step at a strain rate $1.6*10^{-5}$ $s^{-1}$ was too weak to be truly resolved in the solid salt assembly. Experiment Z-5 was performed at 800°C, and strain rates of $1.6*10^{-4}$, $1.6*10^{-6}$, and $1.6*10^{-5}$ $s^{-1}$. Of those steps, only the middle step, at the strain rate $1.6*10^{-6}$ $s^{-1}$, yielded, at 56 MPa differential stress. The middle step was performed from ~9% to ~15% strain, and yielded around 13%. These experiments showed that the strength of the synthetic quartz was greatly influenced by the strain rate, with the strength increasing with faster strain rates (Figure 7).

The microstructures in the thin section from Z-2 are similar to those discussed in the thin section from Z-29 (Figure 8). The undulatory extinction is a bit more visible in this sample, and the water still seems randomly distributed in fluid inclusions. The microstructures from sample Z-5 were overwritten by the last step; the sample is

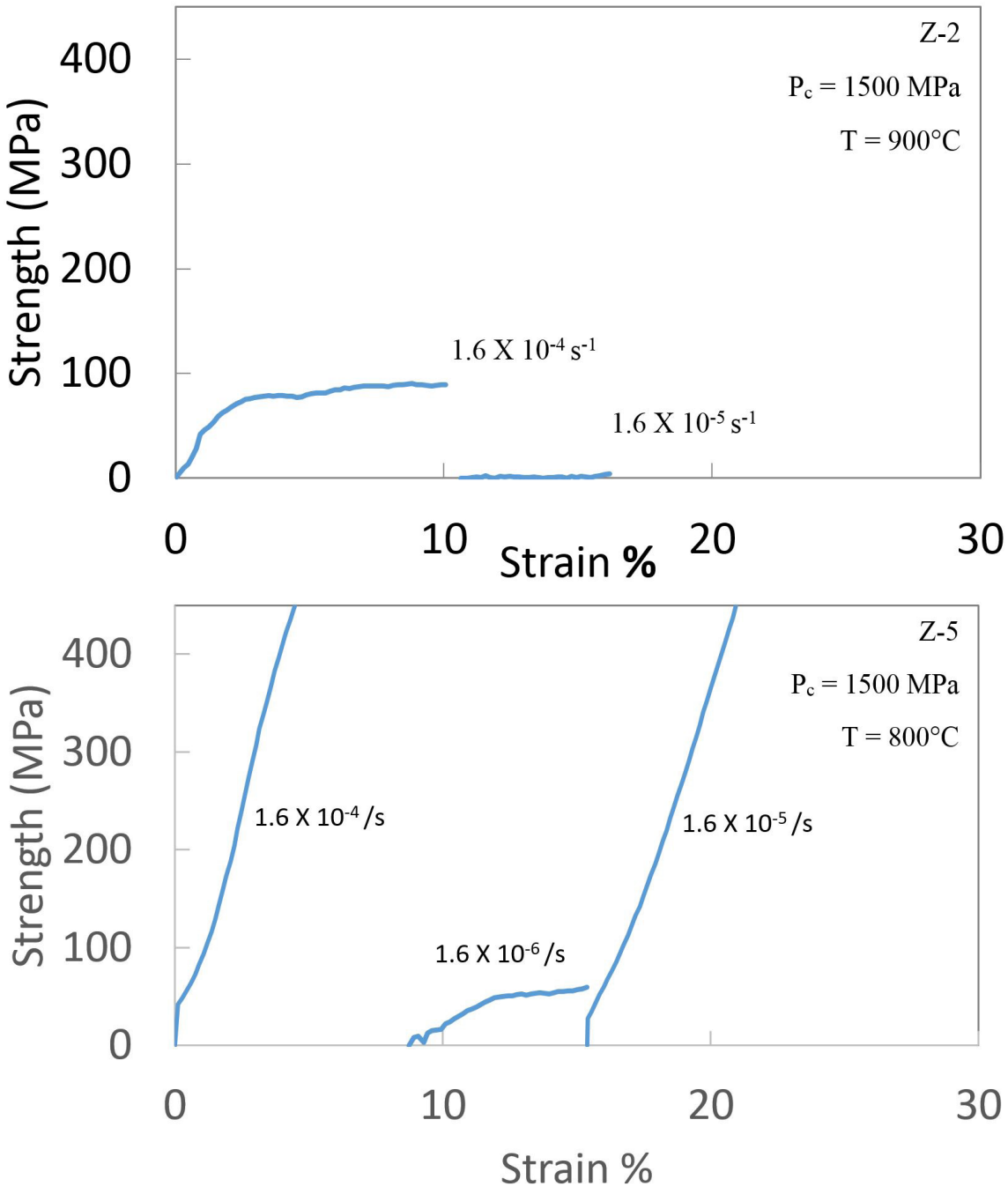


Figure 7. Stress strain curves for experiments Z-2 (top) and Z-5 (bottom). The deformation steps occurring at faster strain rates experienced higher differential stress then the deformation steps at slower strain rates.

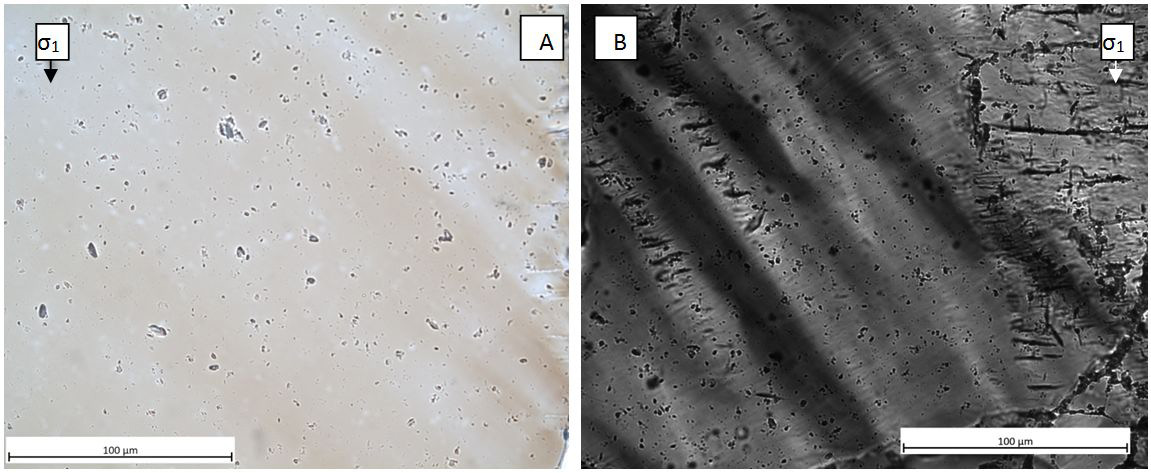


Figure 8. (A) Sample Z-2 (900°C and 16% strain) and (B) sample Z-5 (800°C and 23% strain). Both experiments were performed at a confining pressure of 1.5 GPa, and had strain rate steps at $1.6*10^{-4}$ $s^{-1}$, and $1.6*10^{-5}$ $s^{-1}$, with Z-5 having an additional step at $1.6*10^{-6}$ $s^{-1}$.Both show undulatory extinction, with Z-5 also showing deformation lamellae.

partially recrystallized, and also has many unloading cracks. The image of Z-5 in Figure 8 represents some of the least deformed area of the sample, which shows undulatory extinction. Outside of the recrystallized portions of Z-5, microstructures appear consistent with dislocation creep.

3.2.2 Molten salt experiments Z-23, Z-26, and Z-28

Three strain rate-stepping experiments were performed in molten salt assemblies to measure the lower strengths of samples at the slower strain rates and higher temperatures, which could not be resolved in the solid salt assemblies. Z-23 was performed 900°C and 1500 MPa, after an initial step at 1000°C that proved too weak (<10 MPa) to resolve satisfactorily (Figure 9). Three deformation steps were performed at strain rates of $1.6*10^{-4}$ $s^{-1}$, $6.8*10^{-5}$ $s^{-1}$, and $1.6*10^{-5}$ $s^{-1}$. The total strain was ~19%, with the first well defined step inducing ~4.5% strain, 2% after the yield point at 58 MPa, the second ~3% strain with ~2% after yielding at 40 MPa, and the last step ~4% with ~2.5% after yielding at 29 MPa. The slower strain rates yielded at a lower differential stress than the faster ones (Figure 9).

Experiment Z-26 was performed at a temperature of 800°C, confining pressure of 1500 MPa, and strain rates of $1.6*10^{-6}$ $s^{-1}$, $1.6*10^{-5}$ $s^{-1}$, and $6.8*10^{-6}$ $s^{-1}$. The first deformation step does not appear to have reached a yield point. The second deformation step, at $1.6*10^{-5}$ $s^{-1}$, experienced ~12% strain during that step, and yielded only near the end of the step, at a differential stress of 140 MPa. The mechanical data for the final deformation step was contaminated by the occurrence of a molten salt leak that dissolved the sample; the maximum differential stress experienced was 48 MPa, but it could have been stronger had the salt leak not occurred (Figure 9).

The final strain rate stepping experiment was deformed at a temperature of 850°C confining pressure of 1500 MPa, and five deformation steps at strain rates of $1.6*10^{-4}$ $s^{-1}$,

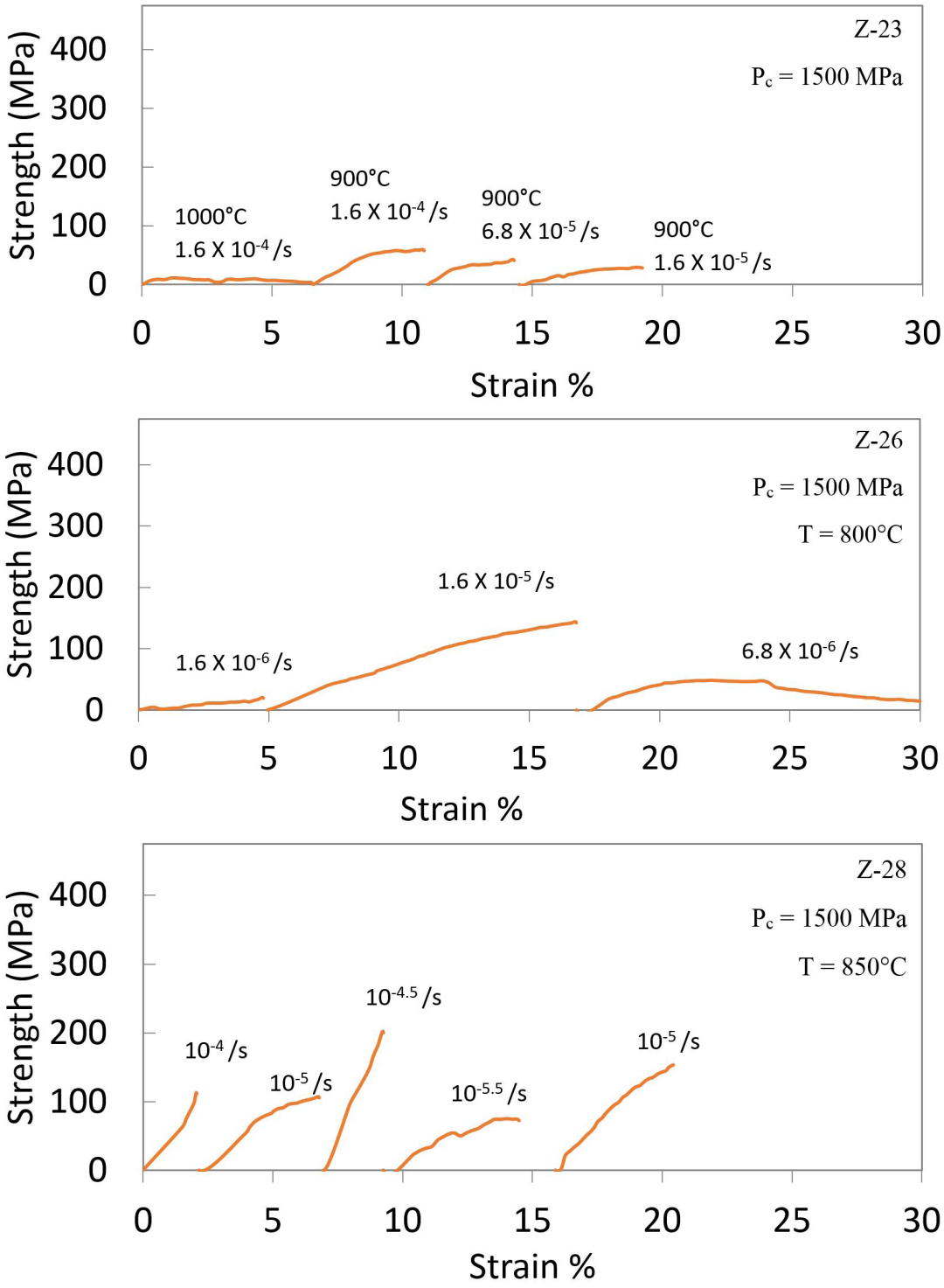


Figure 9. Stress-strain curves for Z-23, Z-26, and Z-28. The deformation steps occurring at faster strain rates experienced higher differential stress then the deformation steps at slower strain rates, and include resolvable differential stresses for multiple deformation steps within an experiment.

$1.6*10^{-5}$ $s^{-1}$, $6.8*10^{-5}$ $s^{-1}$, $6.8*10^{-6}$ $s^{-1}$, and a second $1.6 X 10^{-5}$ $s^{-1}$ step. The first and third deformation steps were too strong for molten salt cell experiments (>250 MPa) and were ended before they yielded. The final step is stronger than the second step at the same conditions. The two steps remaining, the first $1.6 X 10^{-5}$ $s^{-1}$ step and the $6.8 X 10^{-6}$ $s^{-1}$ step are of reasonable strength to measure in the molten salt assembly, and provide some data at an intermediate temperature on the differential stress - strain rate relationship. The first was strained ~4.5% with ~1.5% after yielding, and reached a differential stress of ~106 MPa. The second was strained ~5.5% with ~1.5% after yielding, and reached a differential stress of ~75 MPa.

Sample Z-23 has microstructures similar to those observed in experiments Z-2 / Z-29: at a more macroscopic scale, a slight sweeping undulatory extinction spans the sample. At a smaller scale the microstructures diverge; the fluid inclusions in the sample appear to have started to line up in some places, looking less randomly distributed than samples Z-2 and Z-29 (Figure 10a). Additionally, some deformation lamellae are observed in the sample. Microstructures in the sample are generally consistent with dislocation creep. Z-28 has the most dramatic undulatory extinction of all samples and the start of subgrain boundaries, but not recrystallization has occurred within the sample (Figure 10b).

### 3.3 Pressure stepping experiments

Two experiments were performed to determine the relation of water fugacity to synthetic quartz sample strength. Experiment Z-56 was performed using a molten salt assembly at a temperature of 800°C, a strain rate of $1.6*10^{-6}$ $s^{-1}$, and deformation steps at confining pressures of ~1500 MPa, 900 MPa and 700 MPa. The strength of the sample at each step came out to ~48 MPa (Figure 11). Experiment Z-61 was performed at 750°C and a strain rate of $1.6*10^{-6}$ $s^{-1}$, with three different confining pressure steps: 1500 MPa, 900 MPa, and 680 MPa (Figure 11). These deformation steps show an increase in sample

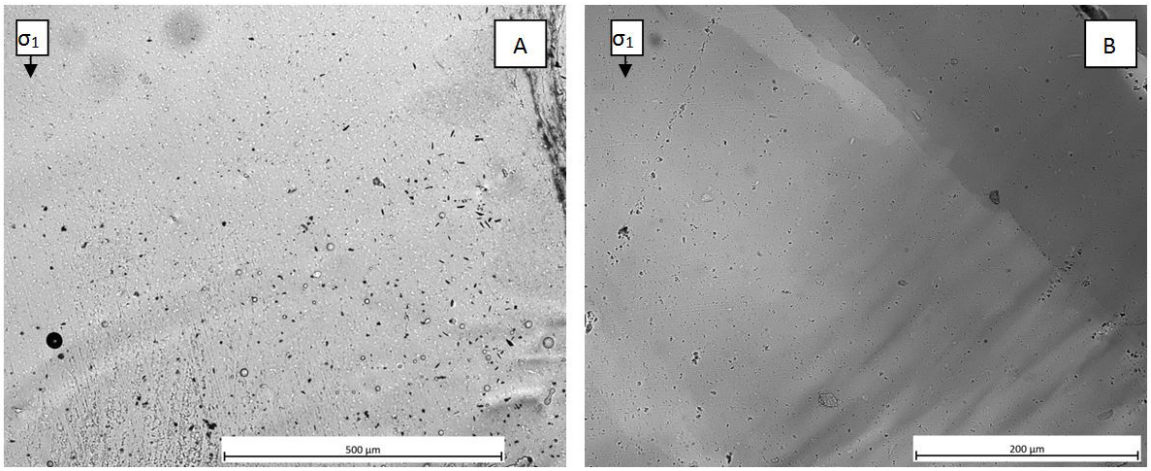


Figure 10. (A) Sample Z-23 (900°C, 19% strain) and (B) sample Z-28 (850°C, 20.5% strain). Both samples were deformed at a confining pressure of 1.5 GPa and had strain rate steps at $1.6*10^{-4}$ $s^{-1}$, $6.8*10^{-4}$ $s^{-1}$, and $1.6*10^{-5}$ $s^{-1}$, with Z-28 also having a strain rate step at $6.8*10^{-6}$ $s^{-1}$. Samples show undulatory extinction and deformation lamellae.

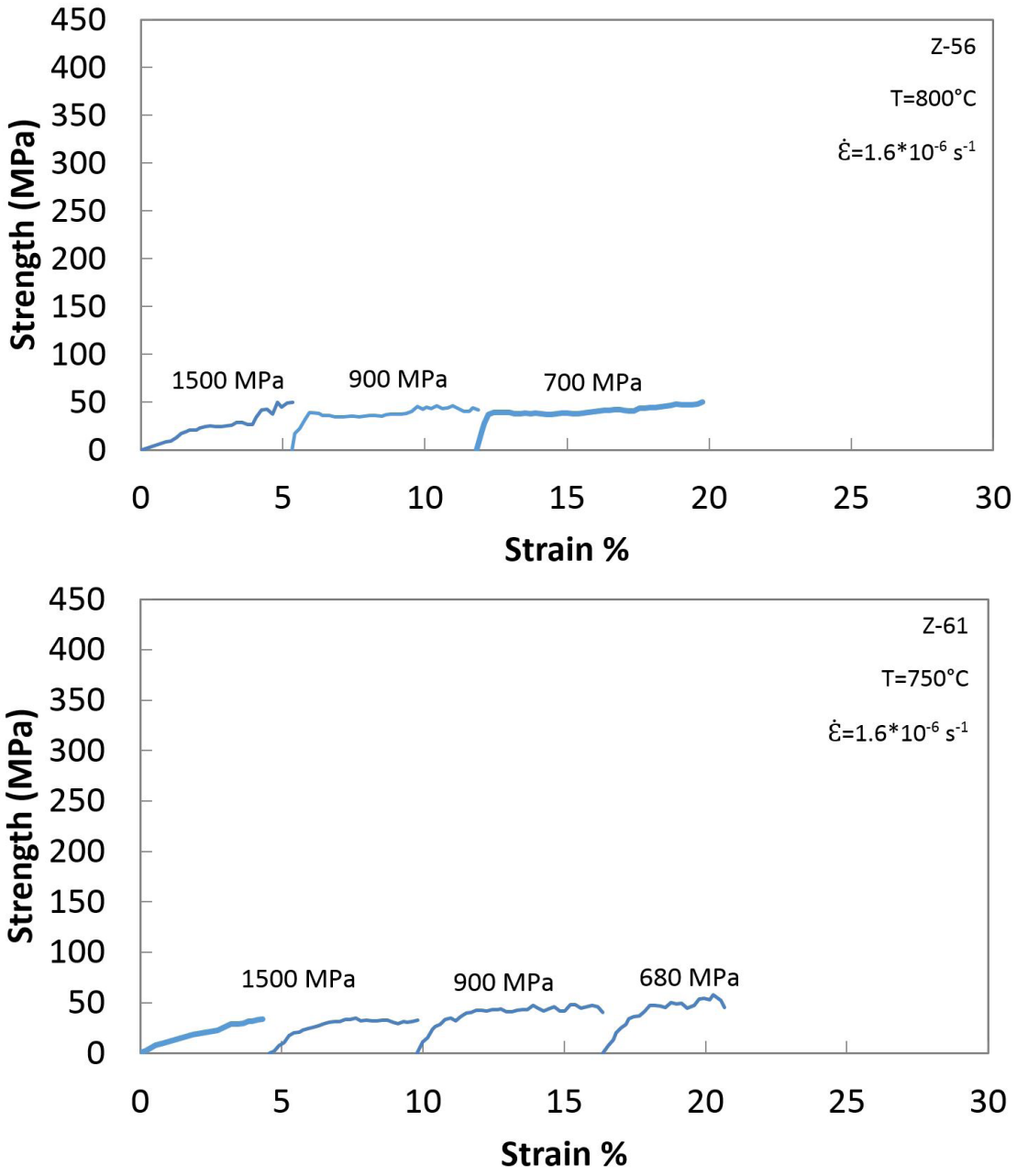


Figure 11. Stress-strain plots for confining pressure-stepping experiments Z-56 and Z-61.

strength at lower confining pressures, with differential stress of 33 MPa, 47 MPa, and 58 MPa corresponding to the 1500 MPa, 900 MPa, and 680 MPa deformation steps respectively.

### 3.4 FTIR Measurements

Water content measured before and after annealing, and after deformation show a change in water content from annealing to be small, though the shape of the FTIR spectra, and therefore form of the water, is seen to change during the annealing process (Figure 12). Unannealed, annealed, and deformed measurements are taken from material cut from the same core during sample preparation. A broad peak from 3800 to 4000 $cm^{-1}$ can be seen in the unannealed sample, which is not present in the annealed or deformed samples. Additionally, a small spike at ~3585 $cm^{-1}$ is present in deformed samples but is much less prominent in the annealed samples.

FTIR measurements on deformed samples show a higher water content than the annealed samples, though the difference is small (Figure 12). Samples taken from nearby each other in the starting crystal have similar water content measurements. Some samples show a change in water content vertically within a sample, but the change is not large enough to rule out thickness changes or random variation. Average water content ranged from <200 to about 1000 $H/10^6$ Si, with wetter samples experiencing much more variation in water content measurements. The standard deviation of the measured water contents comes out to about ±10% of the average water content within the samples with multiple water content measurements. An average FTIR curve for each experiment with FTIR taken is presented in Figure 13. In most cases these were generated using FTIR measurements from different areas in the sample and disregarding abnormally high water content estimates as being not representative of the sample as a whole.

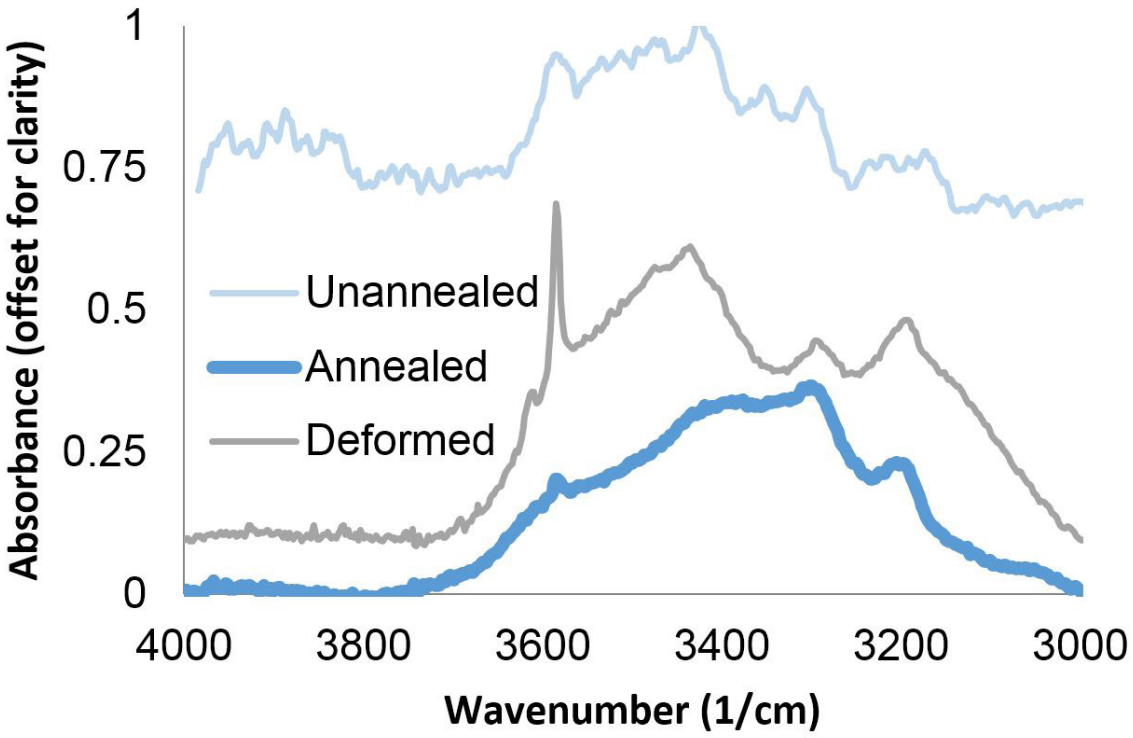


Figure 12. FTIR spectra from sample Z-2 (T=900°C, $P_c$ = 1.5 GPa, strain rate steps at $1.6*10^{-4}$ $s^{-1}$ and $1.6*10^{-5}$ $s^{-1}$, 16% strain). The spectra were normalized to 1 cm sample thickness and the absorbance offset to better show the relative shapes of the spectra.

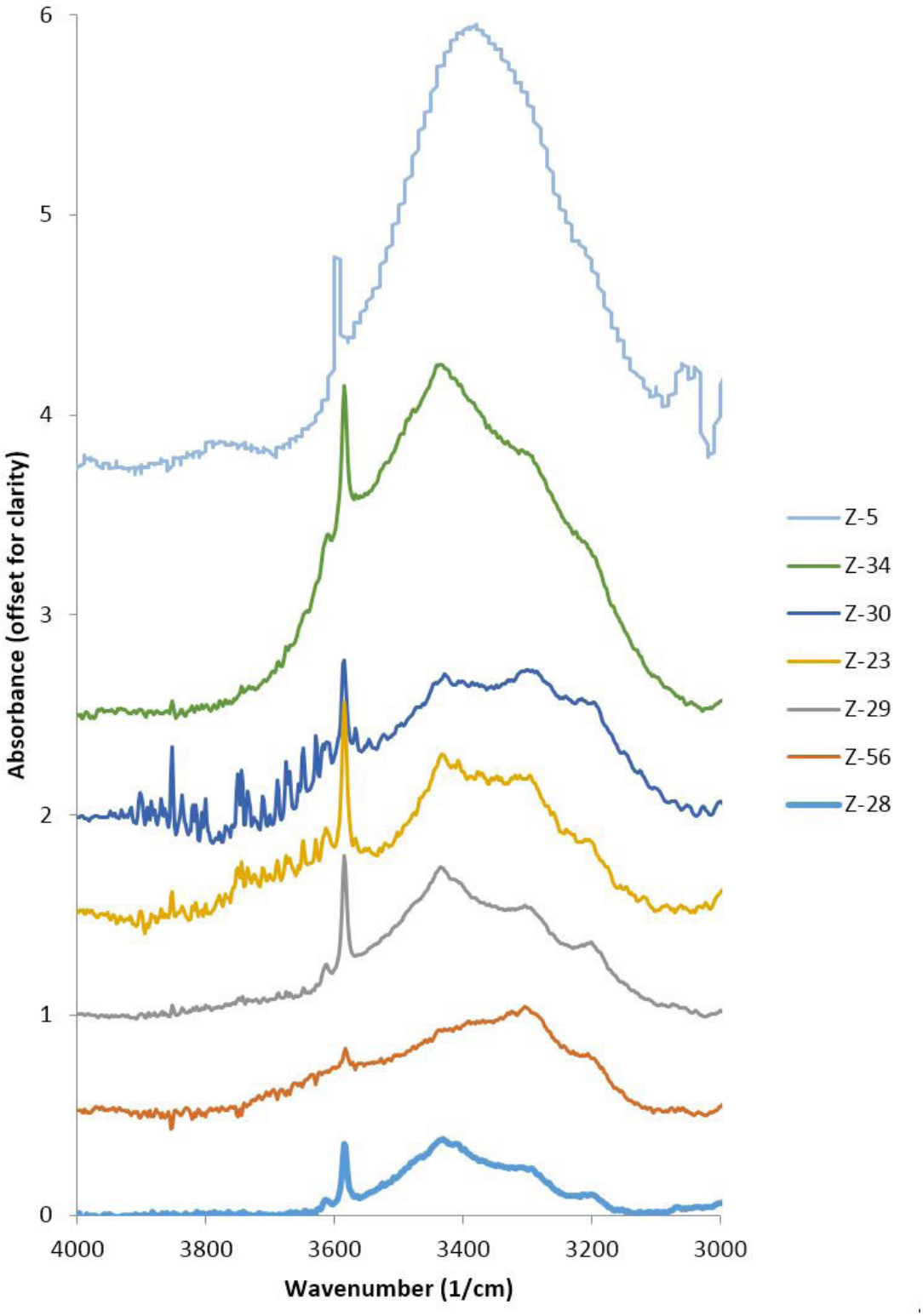


Figure 13. Water content measurements from FTIR sections made from deformed samples. Absorbance values have been offset for clarity.

## 3.5 CIP Measurements

Computer integrated microscopy (CIP) was used in order to determine the c-axis orientation in optical thin sections. CIP programs (Heilbronner and Barrett, 2014) analyzed a series of images from experiment Z-2. Appendix C describes the CIP processes used to generate c-axis azimuth and inclination images (Figure 14). Additional images were also generated through the use of CIP, which describe other properties of the sample, but these images were not used for this study. Of these images, only the azimuth image was necessary to determine the orientation of the c-axis in the 2-D thin section images, which is measured clockwise from the top of the image. In general, the CIP images show that the c-axis orientation was 45° to $\sigma_1$, as expected. From the c-axis orientation, the a-axis orientation can be determined, as it is perpendicular to the c-axis.

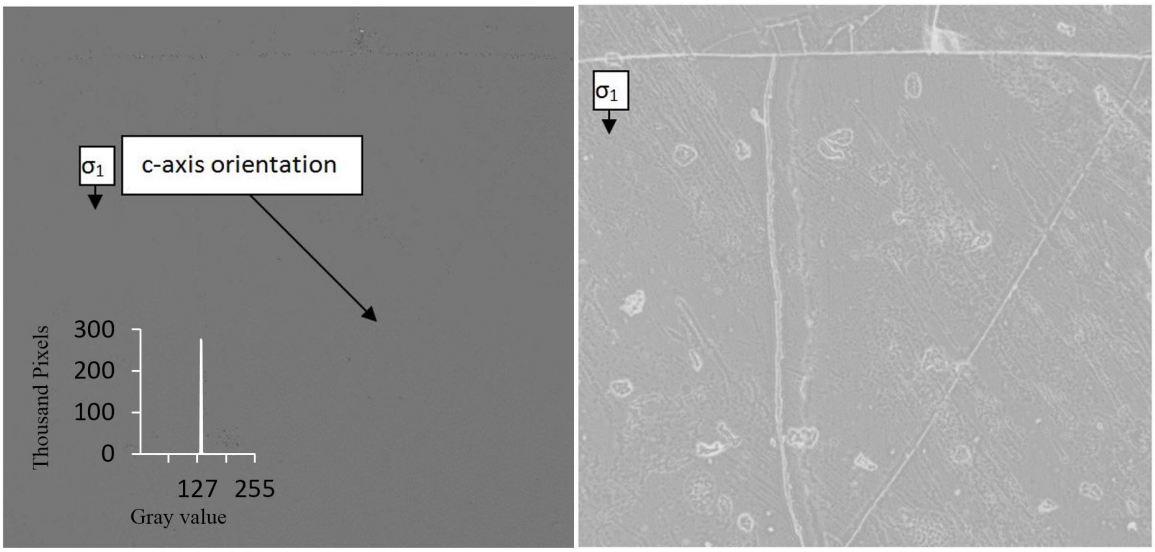


Figure 14. CIP output, taken from sample Z-2. Left: azimuth image; where the shade of gray represents the orientation of the c-axis; in this case the gray value measured 135 (histogram at bottom left) for most of the image, which corresponds to the value of the angle measured clockwise from the top of the image. Right: inclination image; where the shade of gray corresponds to what orientation the c-axis is rotated outside the plane of the image; in this case the value was ~80 for the image.

# CHAPTER IV
# DISCUSSION

Synthetic quartz crystals in the O+ orientation were deformed in this study, and their mechanical data provides insight into the relationship between the strength, strain rate, temperature, water fugacity, and water content for quartz undergoing deformation by dislocation creep. The strain rate stepping experiments show that strength increases with increasing strain rate. The single step experiments at different temperatures show that strength decreases with increasing temperature. The pressure stepping experiments reveal that lower confining pressure results in increased sample strength, associated with water fugacity changes. Finally, the strength variability between samples whose water contents differ according to their FTIR spectra suggest an effect on sample strength caused by differences in water content, with higher water content producing lower strength samples. In addition, the microstructures present in the samples provide information as well, as they vary from experiment to experiment.

## 4.1 Mechanical Data Analysis

A value for the stress exponent (n) of about 3.3 was determined using the results from experiment Z-23 (for which T =900°C, $P_c$=1500 MPa, $\dot{\varepsilon}$=1.6*$10^{-4}$ $s^{-1}$, 6.8*$10^{-5}$ $s^{-1}$, and 1.6*$10^{-5}$ $s^{-1}$). Experiment Z-28, a strain rate stepping experiment at 850°C and 1500 MPa is consistent with the results of Z-23, though Z-28 only produced two useable data points. A combination of points from Z-5, Z-26, and Z-30 (all deformed at T=800°C

and $P_c$=1500 MPa) also produce a comparable value, although there the water content changes among those samples (Figure 15).

Activation energy for the O+ orientation of quartz single crystals was determined to be ~269 ± 30 KJ/mol (Figure 16), based primarily on molten salt experiments Z-23, Z-26 and Z-28, which all have steps at $10^{-5}$ $s^{-1}$, and also on experiments Z-23, Z-29, Z-30, and Z-34, which have steps at $10^{-4.5}$ $s^{-1}$. The comparison of those results was used to determine the relation of the strength and water fugacity to the temperature, which yields a value for the activation energy, Q. Q was taken to be the average of the two values calculated from the two sets of experiments.

The relation between water fugacity and differential stress could be determined using data from experiment Z-61(Figure 17). The resulting slope yields an r/n ratio of about 0.3. Using the value for n calculated in this study, the r/n ratio yields an r value of ~1 (r = 0.996). Water fugacity was determined using Tony Withers' fugacity calculator (Withers, 2016), which uses the Pitzer and Sterner (1994) equation of state for water to determine water fugacity based on pressure and temperature.

The remaining term, A, was calculated for each experiment, including strain rate steps from Z-2, Z-5, Z-23, Z-26, Z-28, Z-29, Z-30, and Z-34, in order to check for changes in A from experiment to experiment. The value for A varied from experiment to experiment, with an average value for log(A) of about 2.1 (~±0.7). Using the varying values of A, the experiments could be normalized to one set of conditions for comparison. The normalized stresses were used to check for a potential linear relation between log(σ) and log(water content), with water content measured in H/$10^6$Si ($r^2$ of 0.8759) (Figure 18). When included into the quartz flow law, it gives a water content exponent of about 1.9 (~±0.2), and a recalculated value for A of ~$10^{-2.75}$. A second check on this value was through comparison between experiment Z-2's $10^{-4}$ $s^{-1}$ step and Z-23's $10^{-4}$ $s^{-1}$ step, as they were performed under similar conditions. Comparing the strength of these two samples

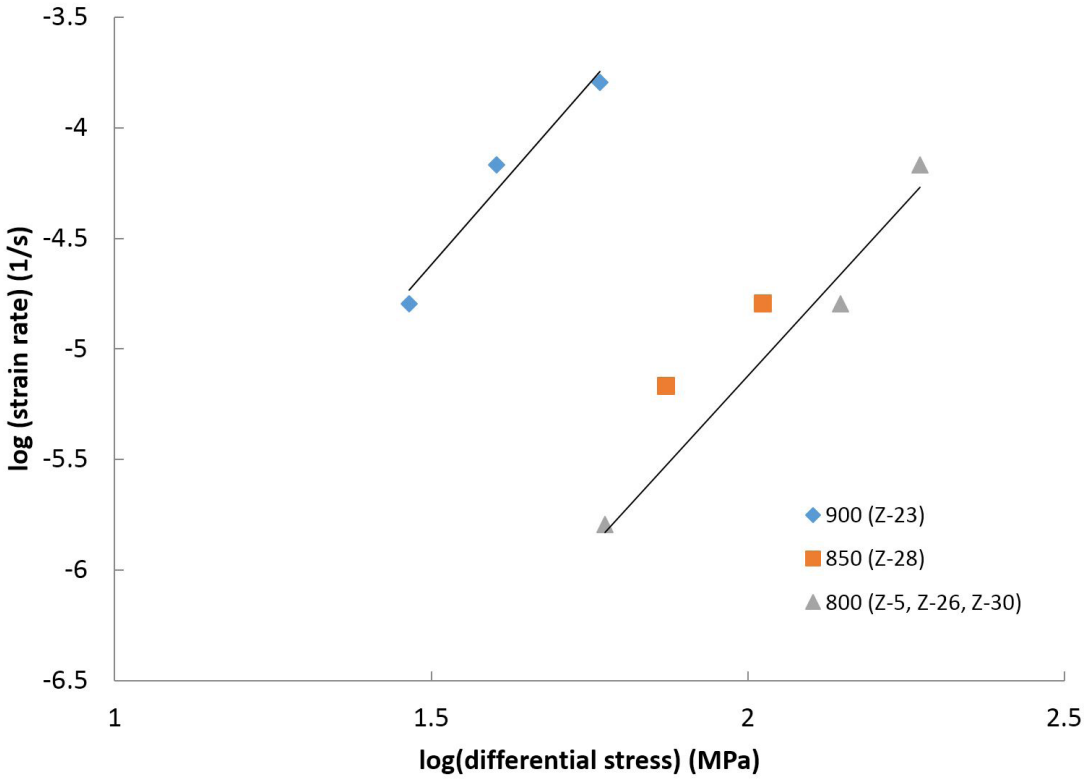


Figure 15. Strength versus strain rate relationship for select samples at different temperatures (in °C). Samples where there is only one data point at that temperature were not included. The slopes of the lines represent n, and give a value of ~3.3.

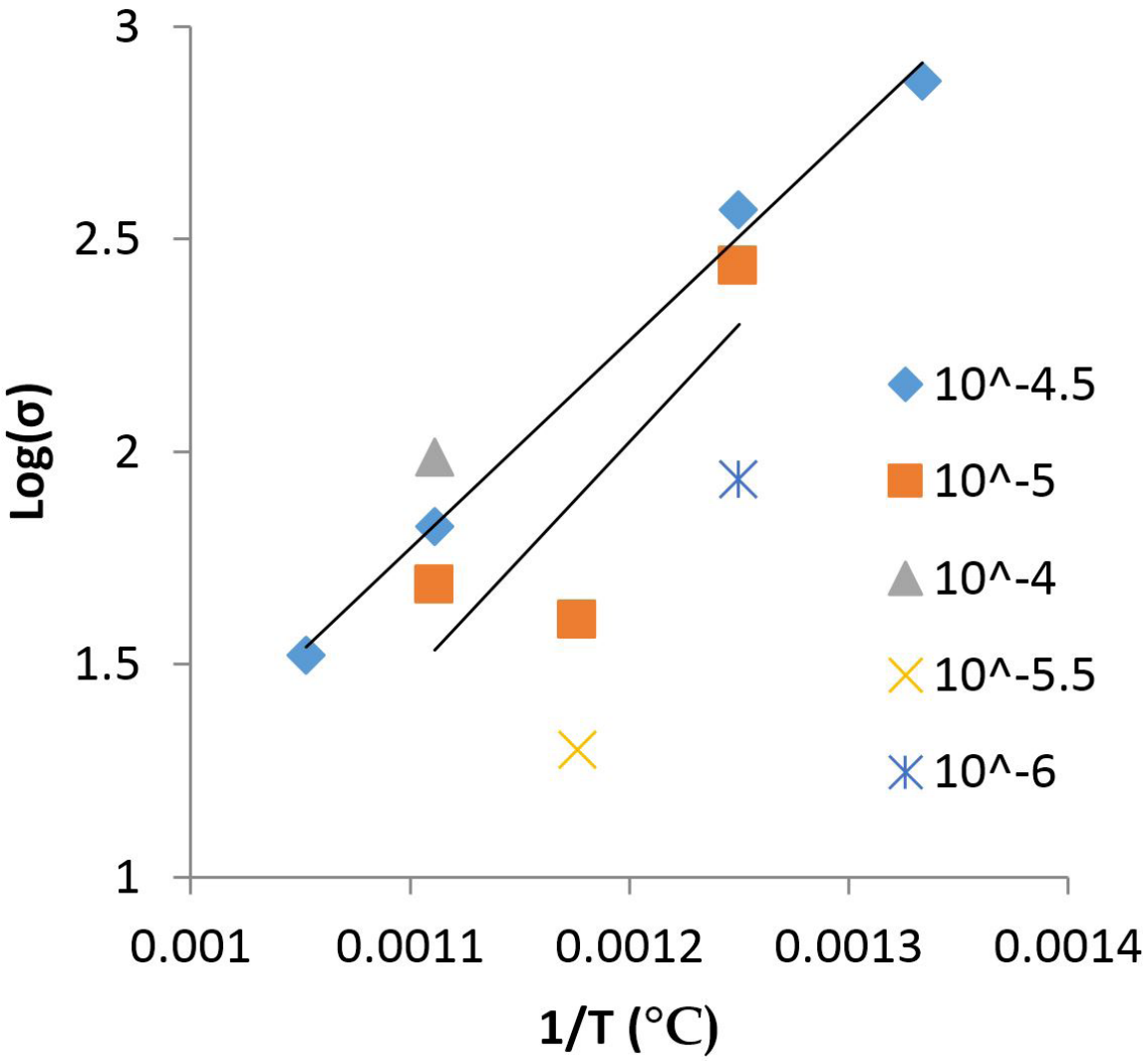


Figure 16. Sample strength versus temperature at different strain rates, corrected for water content and fugacity. The value for Q based on the slopes of these lines comes out to be ~269 kJ/mol.

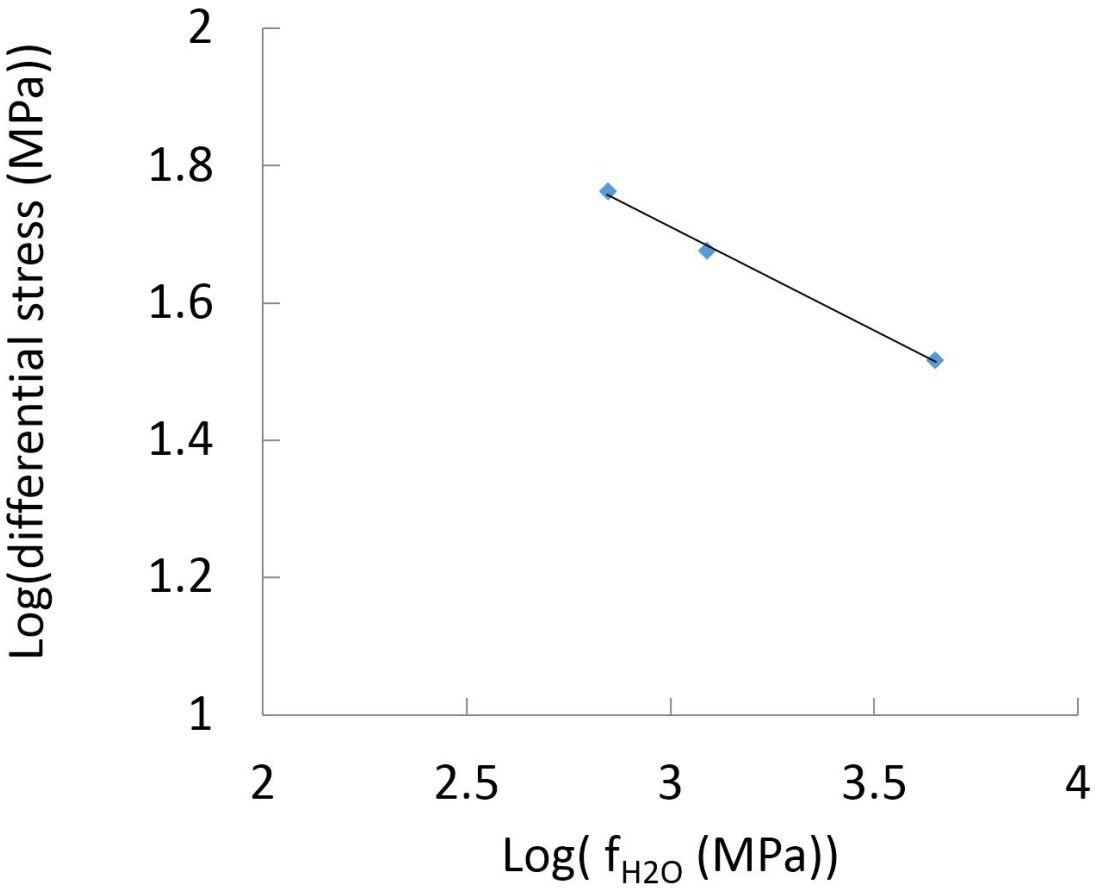


Figure 17. Water fugacity determination using strength measurements from experiment Z-61. The slope of the line represents -r/n which equals about -0.3, giving an r value of about 1.

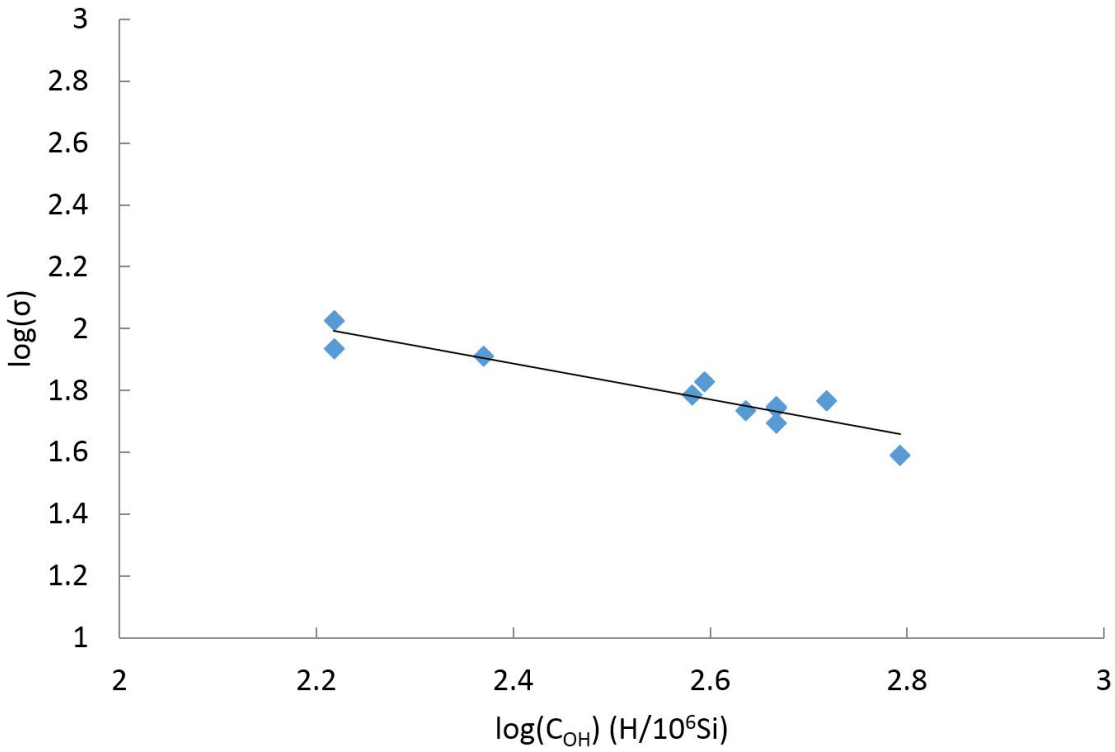


Figure 18. Calculation of the effect of water content on sample strength. Strength was normalized to conditions of 1.5 GPa, 850°C and $1.6*10^{-5}$ /s. The slope of the line represents -z/n, which has a value of about 0.58±0.07, or a z value of 1.9±0.2.

versus their water content yields a water content exponent of ~2. An effect on strength by water content was expected, as samples in this study tended to vary in strength from one experiment to the next, and a high dependence on water content would explain the variation. Water contents used in determining this value range from ~165 H/$10^6$Si to ~621 H/$10^6$Si.

Following the determination of a flow law from these experiments, the different parameters of the equation were examined to see if they were independent of each other. By graphing log(A) vs. log(strength) (for example) and using linear regression to check for a relation between the two, it could be determined that no relation existed, meaning the variables were independent of one another. The results of these graphs for the most part suggest that there was no dependence of any one parameter on any of the other parameters tested (see Appendix D for graphs and further discussion).

Combining all of the values calculated for the flow law parameters, the flow law equation produced using this data set is:

$$\dot{\varepsilon} = 0.00177 * C_{H_2O}^{1.9} * f_{H_2O} * \sigma_{diff}^{3.29} * e^{(-268.6/(R * T))}$$

where $\dot{\varepsilon}$ is strain rate, $C_{H_2O}$ is water content, $f_{H_2O}$ is water fugacity, $\sigma_{diff}$ is differential stress, and T is the temperature. The final standard deviation for log(A) comes out to be about 0.14, or approximately 0.00177±0.0005 for A itself.

## 4.2 Comparisons to Other Studies

The stress exponent (n) has been calculated for O+ oriented quartz (n=3, Linker and Kirby, 1981) and for quartzites (n=4, from Gleason and Tullis, 1995; Hirth et al., 2001; and one set of experiments from Luan and Paterson, 1992; n=2.3 for another set, Luan and Paterson, 1992) in the past, though there is some variability in these measurements.

The activation energy varies as well, with values of 92 kJ/mol (Linker and Kirby, 1981) for O+ quartz, 137 kJ/mol (Gleason and Tullis, 1995; for quartzite samples with ~1-2% melt), 223 kJ/mol (Gleason and Tullis, 1995; for quartzite samples with no melt) 135 kJ/mol (Hirth et al, 2001), and 150 (Luan and Paterson, 1992) for quartzites. Values for the effect of water fugacity exist as well, with Chernak et al. (2009) reporting a water fugacity exponent of between 0.375 and 1, and values of 1.5 for single crystal and 2.5 for quartzite reported by Holyoke and Kronenberg (2013, assuming n=4).

The measured value for n from this study (n=3.3) is comparable to others for quartz crystals and quartzite measurements. Other quartz crystal measurements showed an n value slightly lower but still close to this study's measured value (n=3, Linker and Kirby, 1981). Measurements on quartzite tend to have a higher n value (n=~4 from Gleason and Tullis, 1995, Luan and Paterson, 1992, and Hirth et al., 2001; all performed on quartzite or quartz aggregates), likely due to the presence of quartz grains in harder to strain orientations.

The value measured for Q (~270 kJ/mol) in this study is higher when compared to prior studies of synthetic crystals, which were likely deforming by changing fluid inclusions from gel-like to free water (Q=92KJ/mol, Linker and Kirby, 1981). The value measured in this study is also higher than that measured for quartzite (such as 223 KJ/mol, for samples with no melt present; Gleason and Tullis 1995), likely due to the lack of initial fractures, dislocations, and grain boundaries in a single crystal increasing its strength and thus the energy needed. Other quartzite and quartz aggregate measurements are even lower; with values reported between 135 (Hirth et al, 2001) and 152 (Luan and Paterson, 1992) KJ/mol.

The measured value for a water fugacity exponent from this study is approximately 1, which is similar to that measured by other studies. Recent measurements have determined a value for r/n of 0.37 for milky quartz single crystals, which would give and r of 1.2

using the value of n from this study (Holyoke and Kronenberg, 2013). Other studies have also reported close values for r to that from this study, with low estimates for r such as 0.375 to 1 (Chernak et al., 2009) and higher estimated values around 2 based on quartzite data and experiments (including Kronenberg and Tullis, 1984; Post et al., 1996, and Chernak et al., 2009), corrected by Holyoke and Kronenberg (2013).

The water content effect present in this study is based on water contents in the low to mid hundreds of H/$10^6$Si. This water content is considerably drier than to most quartz studies (roughly one order of magnitude lower). However, since the effect is logarithmic, differences in water content between samples with low water contents will have a larger effect than differences in water content of a similar magnitude in higher water content samples. Studies on quartzite have often used the Black Hills quartzite, which has a water content of ~2500 H/$10^6$Si (Holyoke and Kronenberg, 2013, Gleason and Tullis, 1994, and Chernak et al., 2009). Single crystal studies using milky quartz also have higher water contents, some around ~8000 H/$10^6$Si (Holyoke and Kronenberg, 2013). Other synthetic single crystal studies (such as Linker and Kirby, 1981 and Muto et al., 2011) have water contents similar to the samples used in this study. However, prior studies did not examine the water content range of their quartz samples in respect to the sample strengths.

## 4.3 Applications to nature

The results of this study can be used to examine how a single crystal of quartz would behave under natural deformation conditions. Figure 19 shows how the flow law would be applied in nature, and compares it to common quartzite flow laws. It assumes a pressure (P) gradient calculated by $P=\rho*g*z$ ($\rho$= density of the crust, g= acceleration due to gravity, z= depth), of 25 MPa per km, a temperature gradient of about 25°C/km, a water content comparable to Black Hills Quartzite (2500 H/$10^6$Si), and a strain rate of ~$3X10^{-15}$ $s^{-1}$. The flow law from this study predicts that quartz will transition

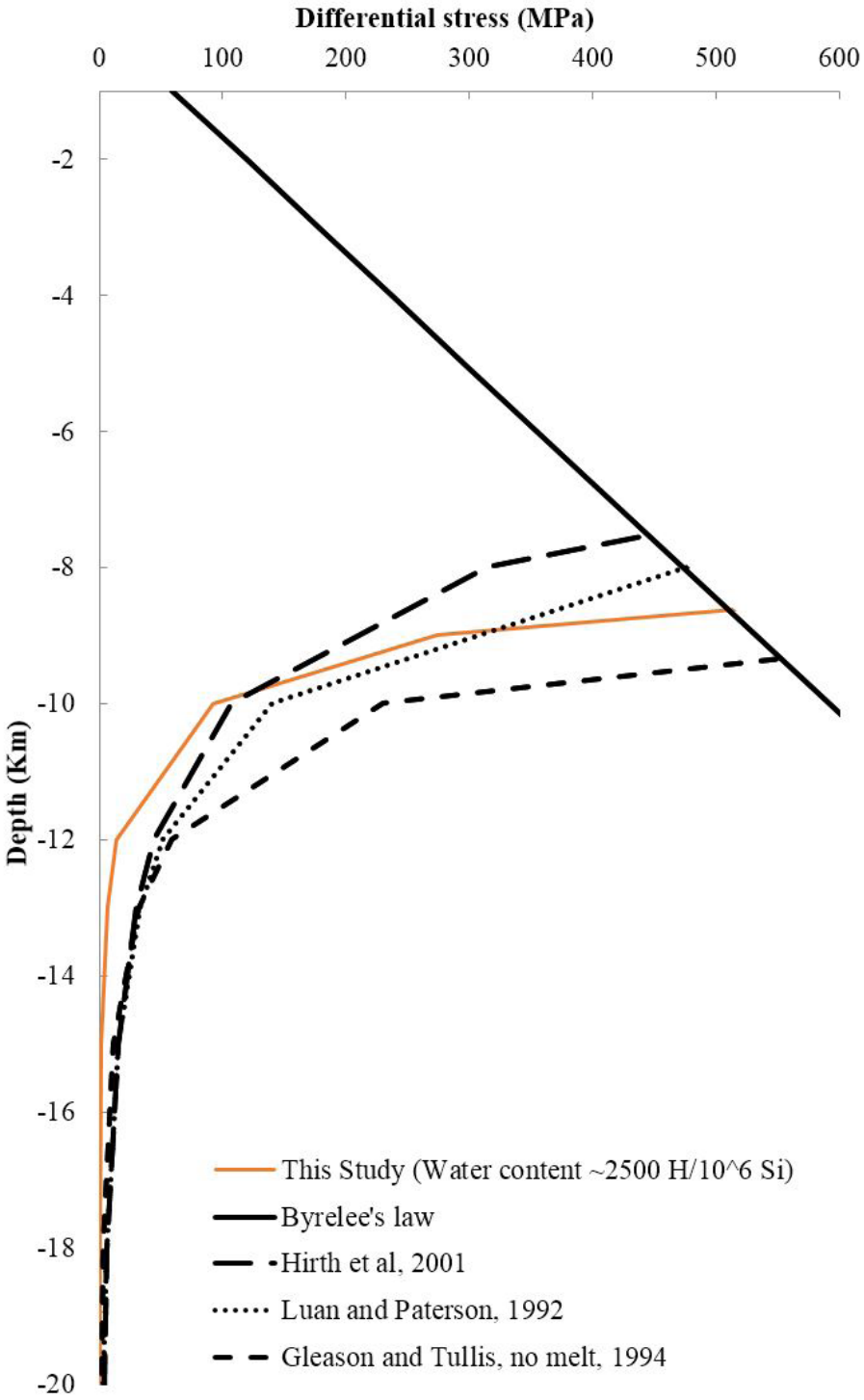


Figure 19. The strength of the lithosphere. The strength of the brittle zone is given by Byerlee's law, while the strength of the ductile zone is given based on the different experimentally determined models for quartzite yield strength (Hirth et al, 2011; Luan and Paterson, 1992; Gleason and Tullis, 1994). The red line represents the model derived from this study.

from brittle to ductile failure mechanisms between 8 and 9 km depth on average. This is deeper than most estimates for quartzites, which translates to the single crystal being a stronger material. Additionally, the flow laws suggest that a single quartz crystal would more rapidly decrease in strength than is shown in formulas for quartzites, becoming weaker than quartzites at depth. The change in relative strength indicates a difference between the synthetic quartz and quartzite. For the portion where the single crystal is stronger, it is likely that the presence of grain boundaries allows processes, such as grain boundary migration, that allow quartzites to deform more easily at higher stresses. In the portion where the quartzite is stronger than the single crystal, the quartzite is likely more influenced by the presence of hard to deform grain orientations present in quartzite that is not the case for a single crystal.

This relationship between flow laws support the findings by Hirth and Tullis (1992), who observed that dislocation climb was not an effective recovery mechanism in their quartz aggregates at low temperatures and fast strain rates (roughly corresponding to >220 MPa differential stress) and the dominant recovery mechanism in that case was grain boundary bulging. Because grain boundary migration does not function for a single quartz crystal, it makes sense that the single crystals would become stronger, as the rate limiting step for deformation becomes the difficulty of dislocation climb. The recovery mechanism change also explains the microstructures visible in the samples from this study. At low stresses, the samples were able to easily deform by dislocation creep, resulting in the mild undulatory extinction visible in samples such as Z-2 and Z-29. At higher strengths, the difficulty of dislocation climb as a recovery mechanism was greater, resulting in more dynamic microstructures, including deformation lamellae and fractures.

An alternative hypothesis is that the water content effect is not represented by a linear relation between strength and water content. While for the purpose of this study it is assumed that the water content can be accounted for by introducing a term of water

content to some power into the flow law, it is possible that the effect water content has on the strength of quartz is more complicated than can be represented by a linear relationship. Some evidence that this may be the case is the changes in water fugacity effect in the different experiments. A future study might consider deforming quartz single crystals of different water contents in pressure stepping experiments, to see if there is a relationship between the water content of the quartz and the effect of water fugacity on the quartz crystals' strength. A possible result would be that the water fugacity exponent increases with increasing water content. This would make sense if low water content prevented the water fugacity from changing with varying confining pressure, and it may be the case that a certain amount of water must be present for the crystal to be 'saturated'. Additionally, if the water content effect is not continuous over all values for water content, it is possible that the equations presented in this study would give weaker values for samples with higher water content than is actually the case, as quartz may stop being affected by additional water after a certain level of saturation. To test this, one would need quartz crystals of a larger range of water content values than were available for this study.

# CHAPTER V

# CONCLUSIONS

Based on my experiments, there are a few things I can conclude about quartz deformation in the O+ orientation. One is that both basal <a> and prism <c> slip systems activate in the O+ orientation after they have reached a moderate amount of percent strain. Another is the stress exponent and activation energy of quartz, for which this study produced values of 3.3 ± 0.2 and 269 ± 30 KJ / (K*mol) respectively, with the effect of water content variability being a possible source of error in the latter. Finally, this study shows that there is a definite effect of water content on the strength of quartz at water contents intermediate between that of dry and milky quartz (specifically in about the 100 to 1000 $H/10^6$ Si range). In this study, it is considered to be another factor in the flow law; however, further study may show that the water content effect changes the characteristics of the deformation and separate flow laws may be need to be considered for dry and wet quartz, with the flow law from this study being a hybridization of the two cases. For example, the possibility exists that a certain amount of water must be present for water fugacity to affect the strength of quartz.

# REFERENCES


Chernak, L.J., Hirth, G., Selverstone, J., Tullis, J., 2009. Effect of aqueous and carbonic fluids on the dislocation creep strength of quartz. Journal of Geophysical Research 114, B04201.

Christie, J. M., Heard, H, C., LaMori, P.N., 1964. Experimental deformation of quartz single crystals at 27 to 30 kilobars confining pressure and 24°C. American Journal of Science. 262, 26-55.

Gleason, G.C., Tullis, J., 1995. A flow law for dislocation creep of quartz aggregates determined with the molten salt cell. Tectonophysics 247, 1–23.

Griggs, D., Blacic, J.D., 1964. The strength of quartz in the ductile regime. EOS Trans. American Geophysical Union 45, 102–103.

Griggs, D.T., Blacic, J.D., 1965. Quartz—anomalous weakness of synthetic crystals. Science 147, 292–295.

Griggs, D. T., Blacic, J.D., Christie, J.M., McLaren, A.C., Frank, F.C., 1966. Hydrolytic Weakening of Quartz Crystals. Science 152, 674.

Hacker, B. R., Yin, A., Christie, J. M., Snoke, A. W., 1990. Differential stress, strain rate, and temperatures of mylonitization in the Ruby Mountains, Nevada: implications for the rate and duration of uplift. Journal of Geophysical Research 95, 8569-8580.

Heilbronner, R., Barrett, S., 2014. Image Analysis in Earth Sciences. Springer-Verlag, Berlin Heidelberg.

Heilbronner, R., Kilian, R., Richter, B., & Marti, S. 2014. Rock Deformation and Microstructure Analysis. https://earth.unibas.ch/micro/ (accessed 2016)

Hirth, G., Teyssier, C., and Dunlap, J. W., 2001. An evaluation of quartzite flow laws based on comparisons between experimentally and naturally deformed rocks. International Journal of Earth Sciences, 90, 77-87. DOI 10.1007/s005310000152

Hirth, G., Tullis, J., 1992. Dislocation creep regimes in quartz aggregates. Journal of Structural Geology 14, 145–159.

Holyoke, C.W., Kronenberg, A.K., 2010. Accurate differential stress measurement using the molten salt cell and solid salt assemblies in the Griggs apparatus with applications to strength, piezometers and rheology. Tectonophysics 494, 17–31.

Holyoke, C.W., Kronenberg, A., 2013. Reversible water weakening of quartz. Earth and Planetary Science Letters 374, 185-190.

Kekulawala, K., Paterson, M., Boland, J., 1981. An experimental study of the role of water in quartz deformation. In: Carter, N.L., Friedman, M., Logan, J.M., Stearns, D.W. (Eds.), Mechanical Behavior of Crustal Rocks: The Handin Volume. American Geophysical Union, Washington, DC, 49–60.

Kekulawala, K.R.S.S., Paterson, M.S., Boland, J.N., 1978. Hydrolytic weakening in quartz. Tectonophysics 46, 1–6.

Kohlstedt, D. L., Evans, B., Mackwell, S. J., 1995. Strength of the Lithosphere: constraints imposed by laboratory experiments. Journal of Geophysical Research, 100, 17587-17602.

Kronenberg, A. K., Lamb, W. M., Luo, Z., Neal, L. A., 2001. Redistribution of water during deformation of milky quartz. EOS Trans. American Geophysics Union, Abstract no. T21C-06.

Linker, M.F., Kirby, S.H., 1981. Anisotropy in the rheology of hydrolytically weakened quartz crystals. In: Carter, N.L., Friedman, M., Logan, J.M., Stearns, D.W. (Eds.), Mechanical Behavior of Crustal Rocks: The Handin Volume. American Geophysical Union, Washington, DC, 29–48.

Luan, F.C., Paterson, M.S., 1992. Preparation and deformation of synthetic aggregates of quartz. Journal of Geophysical Research 97, 301–320.

Muto, J., Hirth, G., Heilbronner, R., Tullis, J., 2011. Plastic anisotropy and fabric evolution in sheared and recrystallized quartz single crystals. Journal of Geophysical Research, 116, B02206, DOI: 10.1029/2010JB007891

Pitzer, K. S., Sterner, S. M., 1994. Equations of state valid continuously from zero to extreme pressures for H2O and CO2. The Journal of Chemical Physics 101, 3111.

Post, A. D., Tullis, J., Yund, R. A., 1996. Effects of chemical environment on dislocation creep of quartzite. Journal of Geophysical Research 101, 22143-22155.

Stewart, E. D., Holyoke, C. W., Kronenberg, A. K., 2013. High pressure deformation experiments using solid confining media and Griggs piston-cylinder methods: Appraisal of stress and deformation in talc assemblies. Tectonophysics 588, 171-178.

Stipp, M., Tullis, J., Behrens, H., 2006. Effect of water on the dislocation creep microstructure and flow stress of quartz and implications for the recrystallized grain size piezometer. Journal of Geophysical Research 111, 201–220.

Stünitz, H., Thust, A., Heilbronner, R., Behrens, H., Kilian, R., Tarantola, A., Fitz Gerald, J., D., 2017. Water redistribution in experimentally deformed natural milky quartz single crystals-Implications for H2O-weakening processes, Journal of Geophysical Research 122, DOI: 10.1002/2016JB013533

Withers, T., 2016, Tony Withers: Fugacity Calculator, http://publish.uwo.ca/~awither5/fugacity/index.htm (accessed 2016)

# APPENDICES

# APPENDIX A

# EXPERIMENTS

The following appendix contains a list of experiments performed during this study. This includes both those used in this study and those that were not included in the determination of the flow law for various reasons.

Table A1. List of experiments and experimental conditions performed during this study.

| Experiment | Solid or Molten assembly | Confining Pressure (MPa) | Temperature (°C) | Strain Rate ($s^{-1}$) | Strain % | Strength (MPa) | Water Content ($H/10^6$ Si) | Used in study | Comments & Microstructures |
|---|---|---|---|---|---|---|---|---|---|
| Z-2 | Solid | 1500 | 900 | $1.6X10^{-4}$ | 10.07 | 88 | 234 | Yes | Fits dataset when corrected for water content |
| | | | | $1.6X10^{-5}$ | 16.18 | 3 | | No | Probably too weak to be reliable, microstructures include undulatory extinction, deformation lamellae |
| Z-5 | Solid | 1500 | 800 | $1.6X10^{-4}$ | 8.74 | >750 | 432 | No | Sample was recrystallized, although since the measurable step fits in the dataset, recrystallization probably occurred in the last step |
| | | | | $1.6X10^{-6}$ | 15.37 | 56 | | Yes | |
| | | | | $1.6X10^{-5}$ | 22.73 | >600 | | No | |
| Z-9 | Solid | 1500 | 850 | $1.6X10^{-6}$ | 5.71 | BDL | 331 | No | 3rd step probably too strong to be the proper deformation mechanism, final step's strength probably increased due to previous step, sample recrystallized in center portion, not at edges. |
| | | | | $1.6X10^{-5}$ | 19.22 | 239 | | | |
| | | | | $1.6X10^{-4}$ | 32.96 | 997 | | | |
| | | | | $1.6X10^{-6}$ | 66.29 | 72 | | | |
| Z-10 | Solid | 1500 | 900 | $1.6X10^{-4}$ | - | - | 360 | No | Strain relaxation attempt, result recrystallized, strange FTIR measurements. First step was too close to the sample to measure the hit point, and did not yield. |
| | | | | | 8.41 | >220 | | | |
| | | | 1000 | | 18.72 | >190 | | | |
| Z-12 | Solid | 1500 | 900 | $1.6X10^{-4}$ | 12.81 | >400 | 470 | No | Strain relaxation attempt, similar recrystallization and FTIR measurement |
| | | | 800 | | 18.27 | >500 | | | |
| Z-13 | Solid | 1500 | 800 | $1.6X10^{-6}$ | 8? | See comment | - | No | Recorder wasn't running during first step, so strain is an estimate. The thermocouple failed during the low confining pressure step. Strength too low to measure |
| | | | | | 16? | | | | |
| | | 1000 | | | 22? | | | | |
| Z-15 | Solid | 1500 | 900 | $1.6X10^{-5}$ | 8.85 | See comment | 207, see comment | No | Ftir sample broke apart, water content may have been larger than listed (given is unannealed water content). Strength of first step too low to measure in solid salt cell. |
| | | | | $6.8X10^{-5}$ | 17.7 | 119 | | | |
| | | | | $1.6X10^{-4}$ | 26.28 | >384 | | | |
| | | | | $1.6X10^{-5}$ | 31.86 | 123 | | | |
| Z-20 | Solid | 1500 | 800 | $6.8X10^{-6}$ | 9.03 | See comment | 989 | No | Sample is recrystallized in places, and the strength is too low for the first three steps compared to the expected values (the first two are too low to measure), while the last step is stronger, so it is unlikely that it is deforming by the expected deformation mechanism at that point. |
| | | | | $1.6X10^{-6}$ | 14.94 | | | | |
| | | | | $1.6X10^{-5}$ | 27.4 | 19 | | | |
| | | | | $6.8X10^{-5}$ | 48.18 | 242 | | | |
| Z-23 | Molten | 1500 | 1000 | $1.6X10^{-4}$ | 6.5 | 7 | 464 | No | Probably too weak to be reliable |
| | | | 900 | $1.6X10^{-4}$ | 11.03 | 58.4 | | Yes | Microstructures: sample shows some undulatory extinction. |
| | | | | $6.8X10^{-5}$ | 14.5 | 40.2 | | | |

Table A1 (cont'd.). List of experiments and experimental conditions performed during this study.

| | | | | | | | | | |
|---|---|---|---|---|---|---|---|---|---|
| Z-23 | Molten | 1500 | 900 | $1.6X10^{-5}$ | 19.22 | 29.2 | 464 | Yes | |
| Z-26 | Molten | 1500 | 800 | $1.6X10^{-6}$ | 4.94 | 26 | 393, see comment | No | Salt leak weakened sample toward end; first step's strength is obscured by confining pressure fluctuations and is not reliable enough to use in determining the equation. Water content is estimated by an average of nearby sample water contents. |
| | | | | $1.6X10^{-5}$ | 16.8 | 140 | | Yes | |
| | | | | $6.8X10^{-6}$ | 33.63 | 48 | | No | |
| Z-28 | Molten | 1500 | 850 | $1.6X10^{-4}$ | 2.2 | >125 | 165 | No | Undulatory extinction occurs both parallel to and perpendicular to c axis orientation. Sample seems unusually dry compared to others, but also appears stronger. |
| | | | | $1.6X10^{-5}$ | 7 | 106 | | Yes | |
| | | | | $6.8X10^{-5}$ | 9.26 | >200 | | No | |
| | | | | $6.8X10^{-6}$ | 14.5 | 74.5 | | Yes | |
| | | | | $1.6X10^{-5}$ | 20.43 | >150 | | No | |
| Z-29 | Molten | 1500 | 950 | $6.8X10^{-5}$ | 10.92 | 28 | 382 | Yes | Undulatory extinction |
| Z-30 | Solid | 1500 | 800 | $6.8X10^{-5}$ | 19.3 | 187 | 523 | Yes | Undulatory extinction, fractures |
| Z-34 | Solid | 1500 | 750 | $6.8X10^{-5}$ | 14.3 | 283 | 621, see comment | Yes | Undulatory extinction, fractures Water measurements showed high variability. |
| Z-37 | Molten | 1500 | 950 | - | - | - | - | No | Recorder was not functioning properly |
| Z-38 | Solid | 1500 | 750 | $6.8X10^{-5}$ | 8.1 | >800 | - | No | Mechanical data did not match expected values, so no further study of the sample was done. |
| | | | | $1.6X10^{-5}$ | 14.7 | 133 | | | |
| | | | | $1.6X10^{-6}$ | 21 | 10 | | | |
| | | | | $6.8X10^{-6}$ | 25.1 | 60 | | | |
| | | | | $1.6X10^{-5}$ | 34.5 | 350 | | | |
| Z-39 | Solid | 1500 | 850 | $1.6X10^{-5}$ | 7.74 | See comment | - | No | Strength too low to measure in the solid salt cell. |
| | | | | $6.8X10^{-5}$ | 14.77 | 79 | | | Mechanical data did not match expected values, so no further study of the sample was done. |
| | | | | $1.6X10^{-4}$ | 35.4 | 458 | | | |
| | | | | $6.8X10^{-5}$ | 41.1 | 33 | | | |
| Z-40 | Molten | 1500 | 950 | $6.8X10^{-5}$ | 3.88 | 48 | - | No | Mechanical data did not match expected values, so no further study of the sample was done. |
| | | | | $1.6X10^{-4}$ | 9.45 | 225 | | | |
| Z-42 | Solid | 1500 | 800 | $1.6X10^{-6}$ | 5.33 | See comment | - | No | Sample too weak for solid salt assembly to measure. Additionally, strength obscured by variations in the confining pressure. |
| | | | | | 9.97 | | | | |
| | | 800 | | | 14.93 | | | | |
| | | 600 | | | 20.74 | | | | |
| Z-48 | Molten | 1500 | 850 | $6.8X10^{-6}$ | 6.62 | 15 | - | No | Partially dissolved by salt leak, all strength measurements are suspect. Water content measurements not taken due to salt leak. |
| | | | | $6.8X10^{-5}$ | 12.7 | 131 | | | |
| | | | | $1.6X10^{-5}$ | 15.1 | 83 | | | |

Table A1 (cont'd.). List of experiments and experimental conditions performed during this study.

| | | | | | | | | | |
|---|---|---|---|---|---|---|---|---|---|
| Z-50 | Molten | 1500 | 800 | $1.8X10^{-6}$ | 2.9 | 26 | - | No | Partially dissolved by salt leak, confining pressure would not stay constant, and varied during the steps too much for a confident measurement; strength measurements are suspect and no water content measurement made. |
| | | 860 | | | 5.7 | 29 | | | |
| | | 620 | | | 11.5 | 50 | | | |
| | | 1500 | | | 17 | 11.3 | | | |
| Z-56 | Molten | 1470 | 800 | $1.8X10^{-6}$ | 5.33 | 49 | 286 | Yes | Shows possibility of no water fugacity effect, but also had confining pressure problems. Undulatory extinction, possibly starting to recrystalize |
| | | 910 | | | 11.87 | 46 | | | |
| | | 700 | | | 19.77 | 49 | | | |
| Z-61 | Molten | 1475 | See comment | $1.8X10^{-6}$ | 4.5 | 33 | - | No | Temperature not constant during this step, kept near 750 |
| | | | 750 | | 9.8 | | | Yes | Salt leak weakened sample; sample recovered still somewhat intact, indicating salt leak was likely late in the experiment- water content measurement not taken as a result. |
| | | 900 | | | 16.3 | 47.5 | | | |
| | | 680 | | | 20.6 | 58 | | | |
| | | 1500 | | | 24 | 28 | | No | |

# APPENDIX B

## RECRYSTALLIZATION IN EXPERIMENTS

Not all of the experiments remained single crystals. Recrystallization tended to occur when samples were subjected to faster strain rates, producing higher differential stress, and when strain percents went above ~20%.

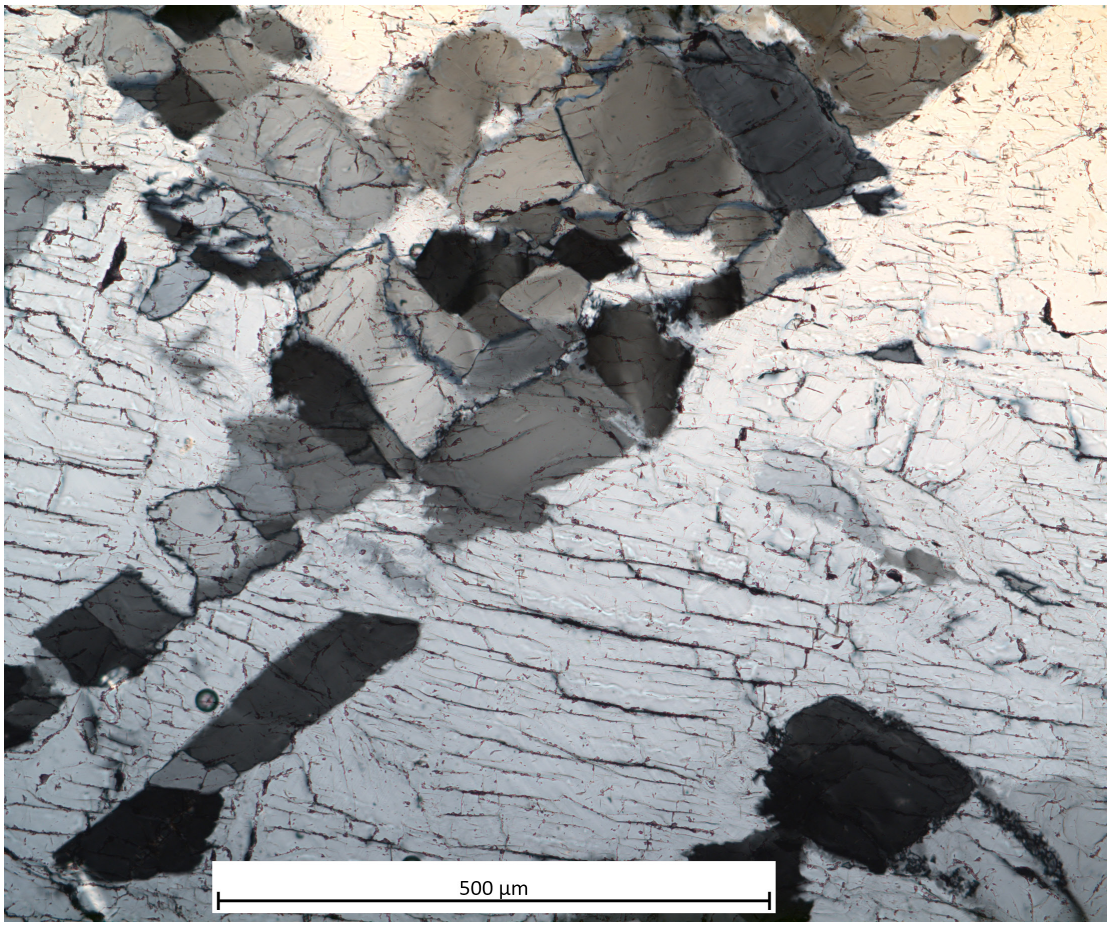


Figure B1. Z-5: 800°C, 1.5 GPa, 3 strain rate steps ($1.6X10^{-4}$, $1.6X10^{-6}$, $1.6X10^{-5}$), total strain ~23%, maximum strength >750 MPa (did not yield for steps 1 and 3). While the data from the one resolvable step of Z-5 fits with the expected results, the sample itself was further deformed past that step, and the results show recrystallization, shown below. An interesting note is that the boundaries of the recrystallized areas tend to occur at 45 degrees (clockwise and counterclockwise) to the principal stress direction; which are the original orientations for the a- and c-axes. This leaves the sample looking sort of like it has the chessboard undulose extinction pattern.

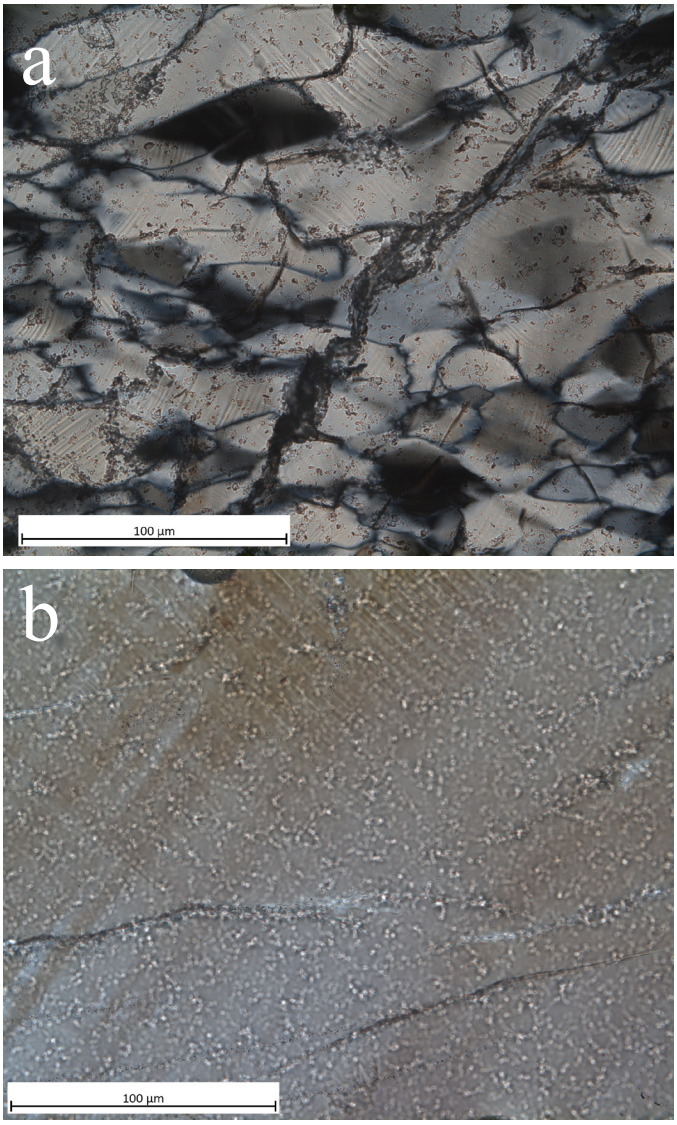


Figure B2. Z-9: 850°C, 1.5 GPa, 4 strain rate steps ($1.6X10^{-6}$, $1.6X10^{-5}$, $1.6X10^{-4}$, $1.6X10^{-6}$), total strain ~66%, maximum strength ~997 MPa. This is another sample that shows recrystallization, with the total strain approaching 66%. (a) The center of Z-9 appears heavily deformed, with recrystallization beginning, in addition to the deformation lamellae. (b) The edges of Z-9 show little deformation, with just the lamellae noticeable. This suggests that the heavy deformation was late in the experiment, and this part of the crystal being loaded; rather, it had been shortened so far as to move this portion out from under the load piston, possibly preserving earlier microstructures.

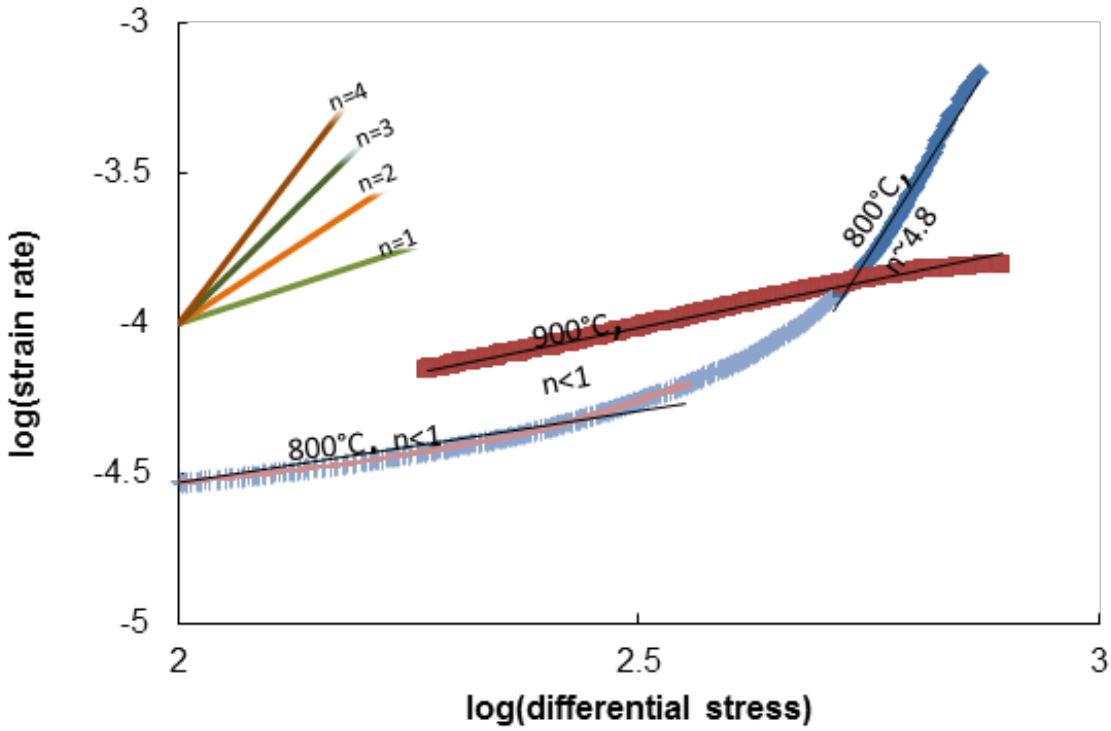


Figure B3. Strain relaxation data from experiments Z-10 (2 steps at 900°C, 1 at 1000°C, 1.5 GPa, total strain ~19%) and Z-12 (2 steps, one at 900°C, another at 800°C, 1.5 GPa, total strain ~18%). In these strain relaxation experiments, the sample was brought up to conditions, deformed quickly (~$10^{-4}$/s strain rate) and then had the motor stopped but not reversed. The load slowly dropped over time, along with the strain rate, as it adjusted to the stress. The strain relaxation data from these experiments were part of an attempt to determine the stress exponent, n, by a different method. The resulting measurements were not consistent with any previously collected data.

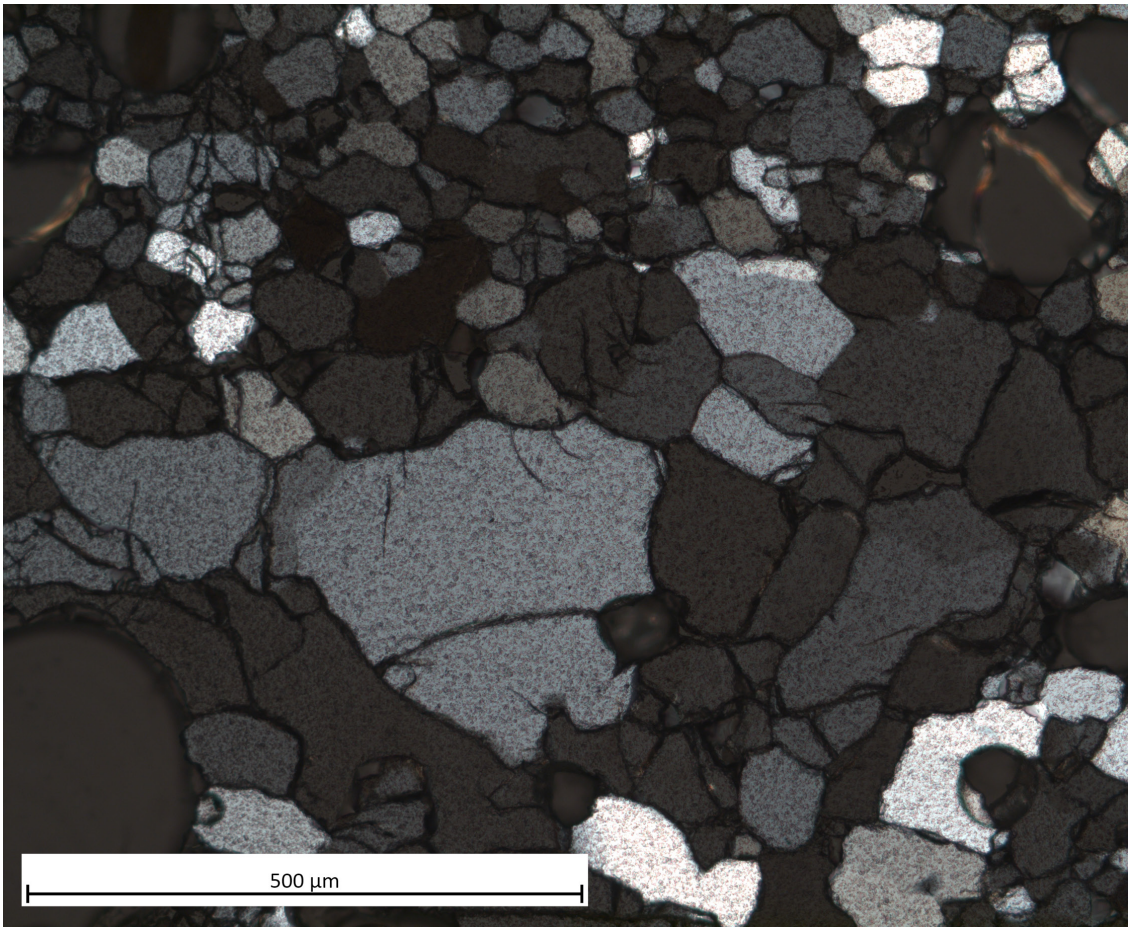

Figure B4. Sample Z-10, showing recrystallization, even more so than Z-5 or Z-9.

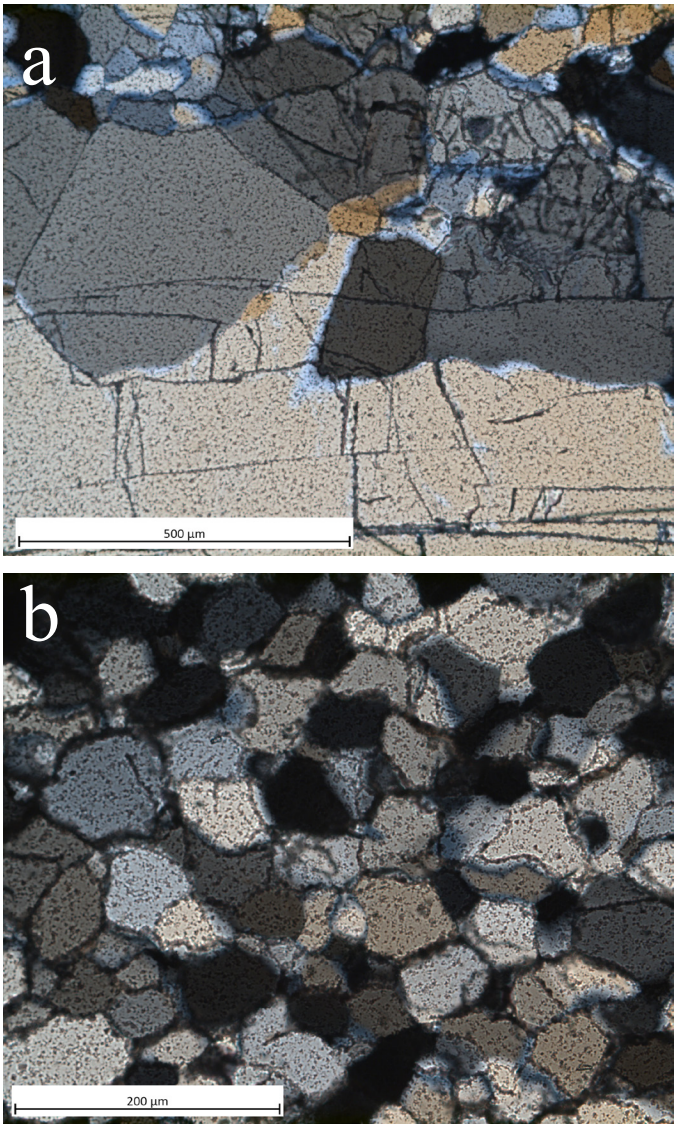


Figure B5. Sample Z-12, with (a) some recrystalization and some material in the original orientation near the edge of the crystal and (b) extensive recrystallization in the center of the sample. The new grains have diameters of about 50 µm.

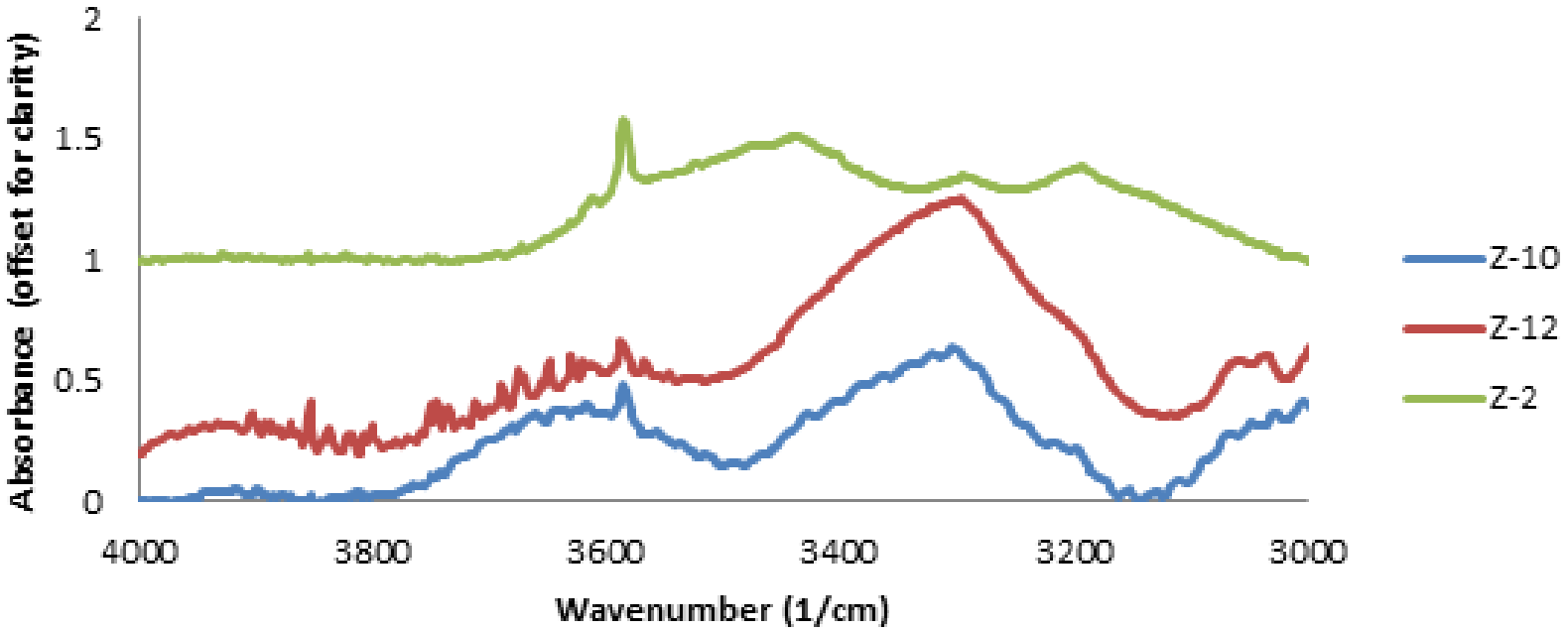


Figure B6. The FTIR spectra from experiments Z-10 and Z-12. The results from experiment Z-2 are shown for comparison. The peaks in the FTIR spectra from Z-10 and Z-12 don't line up well with those of Z-2, or any natural quartz.

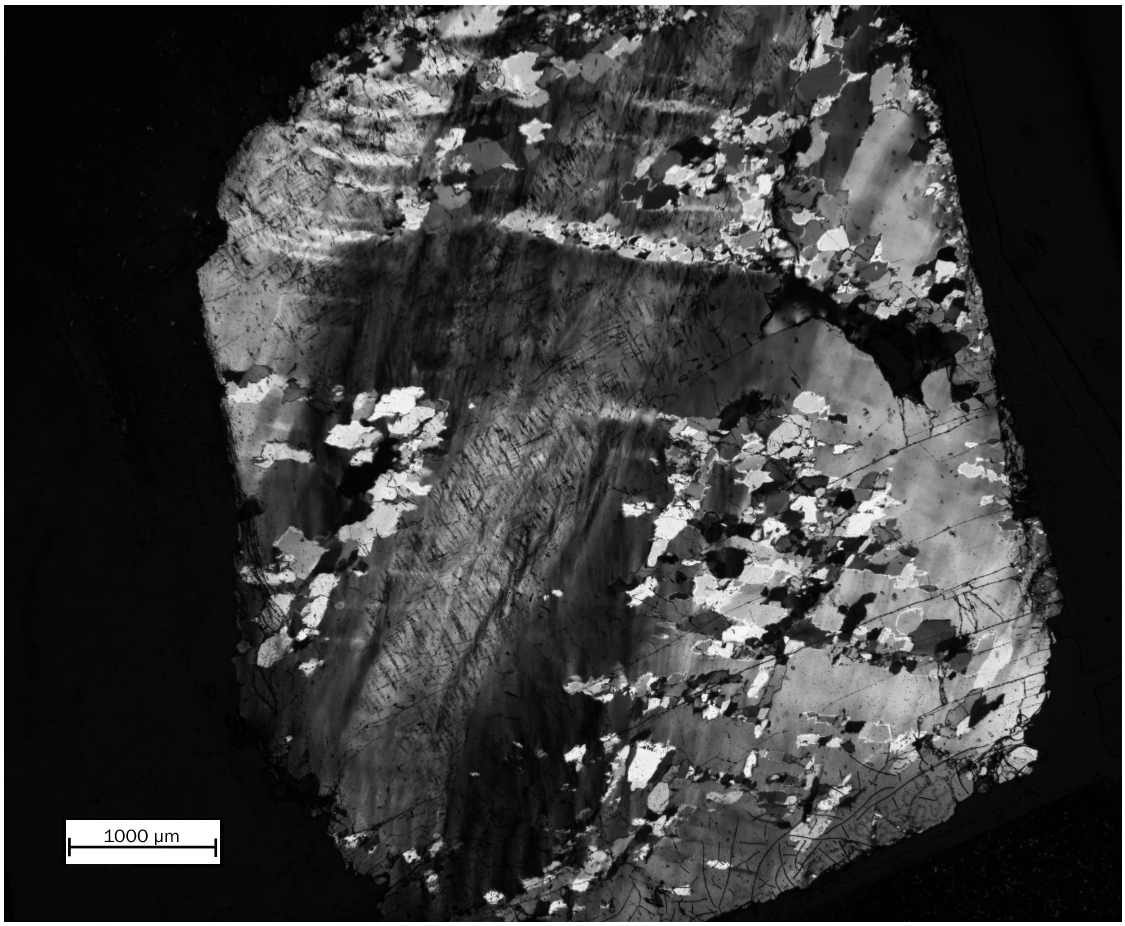


Figure B7. Experiment Z-20: shows some of the chessboard extinction pattern, as well as recrystallization. Features do seem to follow either the a- or c-axis. The measureable steps don't seem to fit the results from the other experiments. All of the strengths measured seem weaker than expected, except for the final strength, which was higher than expected. The high strength of the last step can be attributed to work hardening. Conditions for the experiment were T=800°C, P=1.5 GPa, and 4 strain rate steps ($1.6X10^{-6}$, $6.8X10^{-6}$, $1.6X10^{-5}$, $6.8X10^{-5}$), total strain ~48%, maximum strength ~242 MPa.

# APPENDIX C

## CIP

In order to determine the orientation of the C-axis in my thin section images, I used the CIP processes outlined in Heilbronner and Barret (2014). The images were taken using a Zeiss Axio Scope.A1 polarized light microscope and Axiocam 506 color camera. For each sample CIP was run for, a circular polarized image, a non-polarized image, rotation images (from 0 to 180 degrees, taken every 10 degrees), 4 tilt images (north up, south up, east up, and west up), and two background images (a separate one for the tilt and the rotation images) were taken. Each tilt image was composed of 4 separate images with the microscope focused on different parts of the image.

Images were loaded in Adobe Illustrator in order to save them as grayscale images (the original output from the microscope was in color), and to back rotate the rotation images. The rotation images were taken on a rotating stage rotated counterclockwise, and so the images were rotated clockwise to get them in alignment.

Using Image SXM, the 4 images taken at different focus levels for the tilt images were merged, and were prepared to register together with the rotation images in Image J. Registration of the images was accomplished primarily by using the StackReg macro. In order to ensure successful registration, in addition to rotating the images into alignment beforehand, some cropping was done to eliminate parts of the images that were not shared due to the different area of view of the microscope at different rotations. Additionally, when the images were difficult to align automatically, separate stacks would be aligned by the macro, Align by Line ROI, which brought the images even

closer before running the StackReg macro. A similar process was used to align a circular polarized image and a non-polarized image to the rest of the stack. The nopol image was also processed separately after alignment to produce a mask to remove areas where the quartz would not show the orientation correctly (such as sample edges, fractures, and inclusions). These images were loaded back in Image SXM to convert them to .raw files, which are used as input into the CIP programs.

The CIP programs are cip1a, cip1b, cip2, and cip4, and are run using gfortran. Each program requires a control file; the following are sample control files made for each program during this study, which were modified from those available at https://earth.unibas.ch/micro/, designed for a previous version of the CIP programs (Heilbronner et al. 2014). Only cip1a was required to get the azimuth of the c-axis, and therefore the direction the c-axis should point on my thin sections.

CIP1A:

```
cip---------INPUT----------
1) Title of problem
sample ‘ciptest’ 4 tilts
2a) x- and y dimension
1056,877
2b) no.of tilts,tilt-type (2 tilts: “2,012”=soft-EUP-SUP,”2,134”=stiff-WUP-NUP,etc.,4
tilts:”4,0”=soft,”4,1”=stiff)
4,0
2c) Corrections ROT-bg,TILT-bg,FLARE,cirpol-camera? (0=don’t 1=do)
1,1,1,0
3) Rotation images (Number = N$ROT):
        at 10 degrees
/Users/ejp46/Desktop/CIPsite4tilt/ciptest/input/ciptest2reg2c.tif.010
        at 20 degrees
/Users/ejp46/Desktop/CIPsite4tilt/ciptest/input/ciptest2reg2c.tif.020
        at 30 degrees
/Users/ejp46/Desktop/CIPsite4tilt/ciptest/input/ciptest2reg2c.tif.030
        at 40 degrees
/Users/ejp46/Desktop/CIPsite4tilt/ciptest/input/ciptest2reg2c.tif.040
        at 50 degrees
/Users/ejp46/Desktop/CIPsite4tilt/ciptest/input/ciptest2reg2c.tif.050
        at 60 degrees
/Users/ejp46/Desktop/CIPsite4tilt/ciptest/input/ciptest2reg2c.tif.060
        at 70 degrees
/Users/ejp46/Desktop/CIPsite4tilt/ciptest/input/ciptest2reg2c.tif.070
```

at 80 degrees
/Users/ejp46/Desktop/CIPsite4tilt/ciptest/input/ciptest2reg2c.tif.080
at 90 degrees
/Users/ejp46/Desktop/CIPsite4tilt/ciptest/input/ciptest2reg2c.tif.090
at 100 degrees
/Users/ejp46/Desktop/CIPsite4tilt/ciptest/input/ciptest2reg2c.tif.100
at 110 degrees
/Users/ejp46/Desktop/CIPsite4tilt/ciptest/input/ciptest2reg2c.tif.110
at 120 degrees
/Users/ejp46/Desktop/CIPsite4tilt/ciptest/input/ciptest2reg2c.tif.120
at 130 degrees
/Users/ejp46/Desktop/CIPsite4tilt/ciptest/input/ciptest2reg2c.tif.130
at 140 degrees
/Users/ejp46/Desktop/CIPsite4tilt/ciptest/input/ciptest2reg2c.tif.140
at 150 degrees
/Users/ejp46/Desktop/CIPsite4tilt/ciptest/input/ciptest2reg2c.tif.150
at 160 degrees
/Users/ejp46/Desktop/CIPsite4tilt/ciptest/input/ciptest2reg2c.tif.160
at 170 degrees
/Users/ejp46/Desktop/CIPsite4tilt/ciptest/input/ciptest2reg2c.tif.170
at 180 degrees
/Users/ejp46/Desktop/CIPsite4tilt/ciptest/input/ciptest2reg2c.tif.180
4a) Tilt images (Number = N$TILT):
First East up
/Users/ejp46/Desktop/CIPsite4tilt/ciptest/input/ciptest2reg2c.tif.eup
Second South up
/Users/ejp46/Desktop/CIPsite4tilt/ciptest/input/ciptest2reg2c.tif.sup
Third West up
/Users/ejp46/Desktop/CIPsite4tilt/ciptest/input/ciptest2reg2c.tif.wup
Fourth North up
/Users/ejp46/Desktop/CIPsite4tilt/ciptest/input/ciptest2reg2c.tif.nup
5) Circular polarization (Number = 1):
/Users/ejp46/Desktop/CIPsite4tilt/ciptest/input/ciptest2reg2c.tif.cirpol
6a) Background for ROT etc. images
/Users/ejp46/Desktop/CIPsite4tilt/ciptest/input/ciptest2reg2c.tif.backR
6b) Background for TILT images
/Users/ejp46/Desktop/CIPsite4tilt/ciptest/input/ciptest2reg2c.tif.backT
7) Calibration of program and camera
/Users/ejp46/Desktop/CIPsite4tilt/calib/axio-micro-660-700.CAL
8) Calibration of inclination
/Users/ejp46/Desktop/CIPsite4tilt/calib/incA-incP-20-lin-660-700.LUT
cip---------CIP1results----------
1) Primary result files
max value
/Users/ejp46/Desktop/CIPsite4tilt/ciptest/CIP1A/ciptest.MAX
min value
/Users/ejp46/Desktop/CIPsite4tilt/ciptest/CIP1A/ciptest.MIN
phase of max
/Users/ejp46/Desktop/CIPsite4tilt/ciptest/CIP1A/ciptest.FMAX
phase of min
/Users/ejp46/Desktop/CIPsite4tilt/ciptest/CIP1A/ciptest.FMIN
error

/Users/ejp46/Desktop/CIPsite4tilt/ciptest/CIP1A/ciptest.ERR
tilt indicator
/Users/ejp46/Desktop/CIPsite4tilt/ciptest/CIP1A/ciptest.TXC
tilt indicator 2
/Users/ejp46/Desktop/CIPsite4tilt/ciptest/CIP1A/ciptest.TXA
2) Final result files
azi
/Users/ejp46/Desktop/CIPsite4tilt/ciptest/CIP1A/ciptest.AZI
inc from polarization
/Users/ejp46/Desktop/CIPsite4tilt/ciptest/CIP1A/ciptest.INCP
inc from amplitude
/Users/ejp46/Desktop/CIPsite4tilt/ciptest/CIP1A/ciptest.INCA
edges from polarization
/Users/ejp46/Desktop/CIPsite4tilt/ciptest/CIP1A/ciptest.EDGP
edges from amplitude
/Users/ejp46/Desktop/CIPsite4tilt/ciptest/CIP1A/ciptest.EDGA
absolute misorientation from North (0,90)
/Users/ejp46/Desktop/CIPsite4tilt/ciptest/CIP1A/ciptest.MISN
absolute misorientation from East (90,90)
/Users/ejp46/Desktop/CIPsite4tilt/ciptest/CIP1A/ciptest.MISE
absolute misorientation from up (0,0)
/Users/ejp46/Desktop/CIPsite4tilt/ciptest/CIP1A/ciptest.MISH
absolute misorientation from ref.direction
/Users/ejp46/Desktop/CIPsite4tilt/ciptest/CIP1A/ciptest.MIS-45-52
3) c-axis orientation image (NON-INTERLEAVED)
/Users/ejp46/Desktop/CIPsite4tilt/ciptest/CIP1A/ciptest.COI1a.raw
4) histogram of axi/dip (5 boxes) as grin MENTEX -> INVPIMA
/Users/ejp46/Desktop/CIPsite4tilt/ciptest/CIP1A/ciptest.CPF

CIP1B:

cip---------INPUT----------
1) Title of problem
sample ‘ciptest’ 4 tilts
2a) x- and y dimension
1056,877
3) azi image:
/Users/ejp46/Desktop/CIPsite4tilt/ciptest/CIP1A/ciptest.AZI
4) inc0 images (0-90):
/Users/ejp46/Desktop/CIPsite4tilt/ciptest/CIP1A/ciptest.INCP
5) T-index file (switch where GV > 0):
/Users/ejp46/Desktop/CIPsite4tilt/ciptest/CIP1A/ciptest.TXC
5) T-index file (switch where GV > 0):
/Users/ejp46/Desktop/CIPsite4tilt/ciptest/CIP1A/ciptest.INCA
5) T-index file (switch where GV > 0):
/Users/ejp46/Desktop/CIPsite4tilt/ciptest/CIP1A/ciptest.TXA
8) Calibration of inclination
/Users/ejp46/Desktop/CIPsite4tilt/calib/incA-incP-20-lin-660-700.LUT
9) Stereographic Colour Lookup Table
/Users/ejp46/Desktop/CIPsite4tilt/Colors/CIP-P-standard.CLUT
cip---------CIP1results----------

1) Final result files
/Users/ejp46/Desktop/CIPsite4tilt/ciptest/CIP1B/ciptest.INCP
1) Final result files
/Users/ejp46/Desktop/CIPsite4tilt/ciptest/CIP1B/ciptest.INCA
1) Final result files
/Users/ejp46/Desktop/CIPsite4tilt/ciptest/CIP1B/ciptest.INCPu
1) Final result files
/Users/ejp46/Desktop/CIPsite4tilt/ciptest/CIP1B/ciptest.INCAu
3) histogram of axi/dip (5 boxes) as from MENTEX -> INVPIMA
/Users/ejp46/Desktop/CIPsite4tilt/ciptest/CIP1B/ciptest.CPF

CIP2:

cip---------INPUT----------
1) Title of problem
sample 'ciptest' 4 tilts
2a) x- and y dimension
1056,877
3) Reference direction for misorientation (N=0,90 E=90,90)
45,90
4) Masking for pole figure and orientation image ? (1=yes, 0=no)
1
5) Want misorientation, edge and orientation image ? (1=yes, 0=no)
1,1,1
6) Pole figure correction 1=sin(inc) 2=sin(inc-1/2) 3=-5-95 4=sqrt(), 5=sin(delta)
1
7) Stereographic Colour Lookup Table
/Users/ejp46/Desktop/CIPsite4tilt/Colors/CIP-P-standard.CLUT
cip---------INPUT FILES----------
1) azimuth file
/Users/ejp46/Desktop/CIPsite4tilt/ciptest/CIP1A/ciptest.AZI
2) inclination file
/Users/ejp46/Desktop/CIPsite4tilt/ciptest/CIP1B/ciptest.INCP
3) masking file (0 where o.k. >0 where masked) (different from CIP1 !!!)
/Users/ejp46/Desktop/CIPsite4tilt/ciptest/input/nopolmask.tif
cip---------OUTPUT IMAGES----------
1) edges using 2 neighbours
/Users/ejp46/Desktop/CIPsite4tilt/ciptest/CIP2/ciptest.EDG2s
2) edges using 4 neighbours
/Users/ejp46/Desktop/CIPsite4tilt/ciptest/CIP2/ciptest.EDG4a
3) absolute misorientation from North (0,90)
/Users/ejp46/Desktop/CIPsite4tilt/ciptest/CIP2/ciptest.MISN2
4) absolute misorientation from East (90,90)
/Users/ejp46/Desktop/CIPsite4tilt/ciptest/CIP2/ciptest.MISE2
5) absolute misorientation from UP (0,0)
/Users/ejp46/Desktop/CIPsite4tilt/ciptest/CIP2/ciptest.MISH2
6) absolute misorientation from ref.direction
/Users/ejp46/Desktop/CIPsite4tilt/ciptest/CIP2/ciptest.MIS-45-90
7) c-axis orientation image (NON-INTERLEAVED)
/Users/ejp46/Desktop/CIPsite4tilt/ciptest/CIP2/ciptest.COI2.raw
8) histogram of azi/dip (5 boxes) as from MENTEX -> INVPIMA

/Users/ejp46/Desktop/CIPsite4tilt/ciptest/CIP2/ciptest.CPF2
9) pole figure image (36*36) -> Lazy Pole
/Users/ejp46/Desktop/CIPsite4tilt/ciptest/CIP2/ciptest.PFIG2

CIP4:

cip---------INPUT----------
1) Title of problem
sample 'ciptest' 4 tilts
2a) x- and y dimension
1056,877
3) 4 reference directions for misorientation (N=0,90 E=90,90)
45,52,135,52,45,128,135,128
4) Masking for pole figure and orientation image ? (1=yes, 0=no)
0
5) Want misorientation, edge and orientation image ? (1=yes, 0=no)
1,1,1
6) Pole figure correction 1=sin(inc) 2=sin(inc-1/2) 3=-5-95 4=sqrt(), 5=sin(delta)
1
7) Stereographic Colour Lookup Table
/Users/ejp46/Desktop/CIPsite4tilt/Colors/CIP-P-standard.CLUT
cip---------INPUT FILES----------
1) azimuth file
/Users/ejp46/Desktop/CIPsite4tilt/ciptest/CIP1A/ciptest.AZI
2) inclination file
/Users/ejp46/Desktop/CIPsite4tilt/ciptest/CIP1B/ciptest.INCP
3) masking file (0 where o.k. >0 where masked) (different from CIP1 !!!)
/Users/ejp46/Desktop/CIPsite4tilt/ciptest/input/nopolmask.tif
cip---------OUTPUT IMAGES----------
1) edges using 8 neighbours average
/Users/ejp46/Desktop/CIPsite4tilt/ciptest/CIP4/ciptest.EDG8a
2) edges using 8 neighbours max
/Users/ejp46/Desktop/CIPsite4tilt/ciptest/CIP4/ciptest.EDG8m
3) absolute misorientation from North (0,90)
/Users/ejp46/Desktop/CIPsite4tilt/ciptest/CIP4/ciptest.MISr1_045_052
4) absolute misorientation from East (90,90)
/Users/ejp46/Desktop/CIPsite4tilt/ciptest/CIP4/ciptest.MISr2_135_052
5) absolute misorientation from UP (0,0)
/Users/ejp46/Desktop/CIPsite4tilt/ciptest/CIP4/ciptest.MISr3_045_128
6) absolute misorientation from ref.direction
/Users/ejp46/Desktop/CIPsite4tilt/ciptest/CIP4/ciptest.MISr4_135_128
7) c-axis orientation image (NON-INTERLEAVED)
/Users/ejp46/Desktop/CIPsite4tilt/ciptest/CIP4/ciptest.COI4.raw
8) histogram of azi/dip (5 boxes) as from MENTEX -> INVPIMA
/Users/ejp46/Desktop/CIPsite4tilt/ciptest/CIP4/ciptest.CPF4
9) pole figure image (36*36) -> Lazy Pole
/Users/ejp46/Desktop/CIPsite4tilt/ciptest/CIP4/ciptest.PFIG4

# APPENDIX D

# INDEPENDENCE ANALYSIS

The following are a series of graphs analyzing the different possible relations between the different parameters in the flow law equation I generated in this study. I expected to find that the slope and $r^2$ values were near zero, as that should indicate that the variables are independent, and a change in one doesn't cause a change in the other beyond what is already documented in my formula. However, if there had been a relation between the variables, it could be corrected by iterative calculation of the associated exponents, though this would have moved the equation from being based on the data collected to a more theoretical equation with less of a basis in the actual data. The graphs for A vs. water fugacity and A vs. $\log(e^{-Q/RT})$ look similar because for this subset of my dataset, the confining pressure was the same for all experiments, so water fugacity is only determined by temperature, and the same is true for Q. The graphs also allowed me to look for other relationships; this is an extension of the method I used to find the relationship between water content and strength, and it allowed me to check for a possible relation between strength and the total strain on the sample.

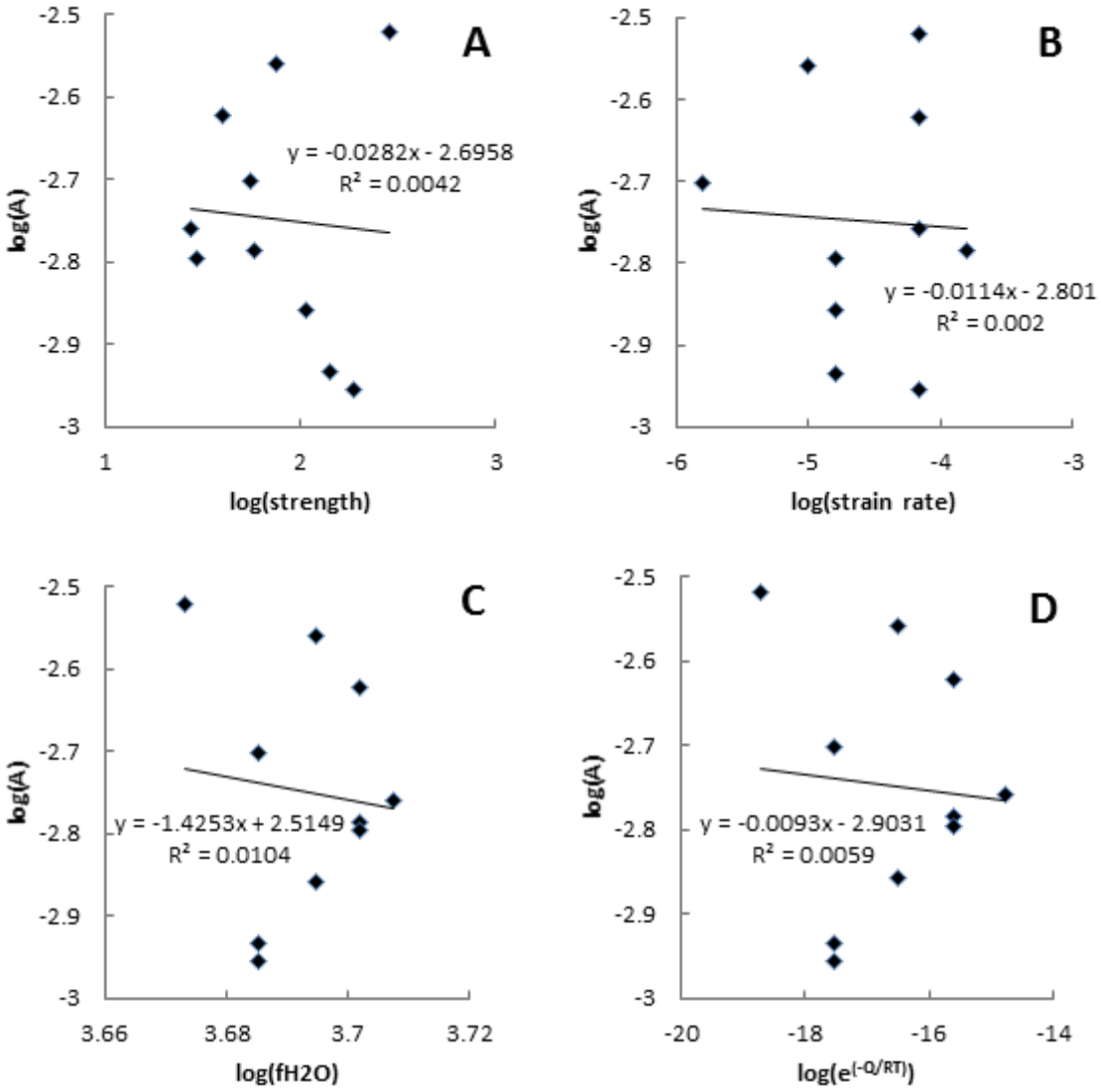
A
y = -0.0282x - 2.6958
R² = 0.0042
log(A)
log(strength)
B
y = -0.0114x - 2.801
R² = 0.002
log(A)
log(strain rate)
C
y = -1.4253x + 2.5149
R² = 0.0104
log(A)
log(fH2O)
D
y = -0.0093x - 2.9031
R² = 0.0059
log(A)
log(e^(-Q/RT))

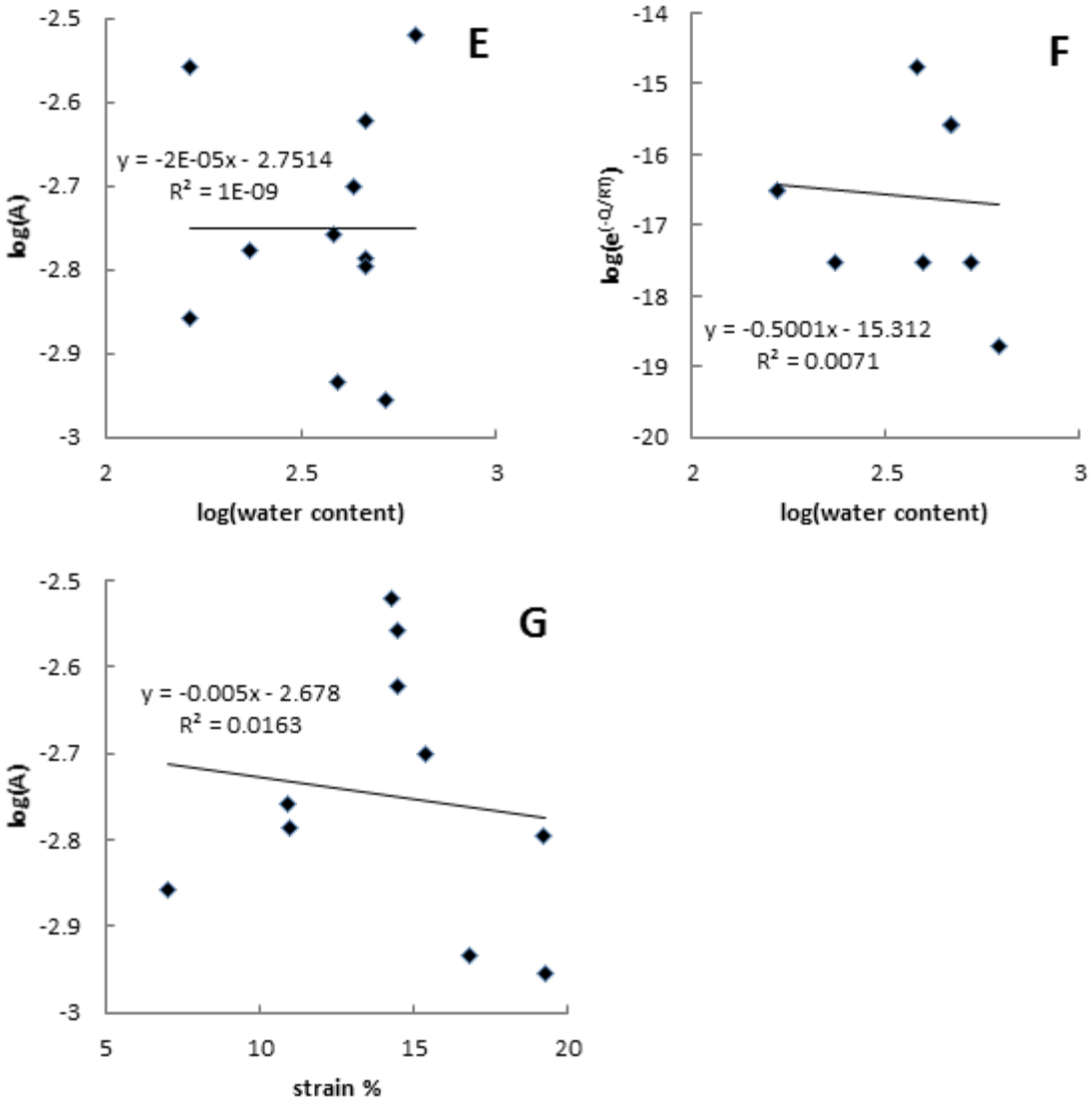


Figure D1. This series of graphs were used to test the different flow law parameters for independence. (A) Graph of sample strength versus A. (B) Graph of strain rate versus A. (C) Graph of water fugacity versus A. (D) Graph of temperature versus A. (E) Graph of water content versus A. These five graphs show that there is no further relationship between the variables that is not already accounted for in the flow law. (F) Graph of water content versus temperature, to see if there was any dependance on the activation energy on the water content; there does not appear to be any based on the graph. (G) Graph of total strain versus A, to see if the sample strength is affected by the amount of strain on the sample; there doesn't appear to be any relation based on the graph of this data set.